

1 **The density of ambient black carbon retrieved by a new method:**  
2 **implications to CCN prediction**

3

4 **Jingye Ren<sup>1,2</sup>, ~~Fang Zhang<sup>2\*</sup>~~, Lu Chen<sup>1</sup>, Jieyao Liu<sup>1</sup>, Fang Zhang<sup>2\*</sup>**

5

6 <sup>1</sup>*College of Global Change and Earth System Science, Beijing Normal University,*  
7 *Beijing 100875, China*

8 <sup>2</sup>*Shenzhen Key Laboratory of Organic Pollution Prevention and Control, School of*  
9 *Civil and Environmental Engineering, Harbin Institute of Technology (Shenzhen),*  
10 *518055 Shenzhen, China*

11

12

13

14

15

16

17 **\*Correspondence to: Fang Zhang ([zhangfang2021@hit.edu.cn](mailto:zhangfang2021@hit.edu.cn))**

18

19

20

21

22

23

24

25 **Abstract.**

26 The effective density of black carbon (BC) is a crucial factor relevant to its aging  
27 degree that would add uncertainty in evaluating its climate effect. Here, we have  
28 developed a new method to retrieve the effective density of internally mixed BC in the  
29 atmosphere combining field observations conducted ~~during from~~ 15 November ~~to~~ 14  
30 December 2016 in urban Beijing with the Köhler theory. The uncertainty of the retrieval  
31 method was evaluated within  $\pm 30\%$ , which ~~is was~~ primarily caused by assumptions  
32 ~~of on both~~ the hygroscopic parameter of organics and the ~~fraction proportional~~  
33 ~~distribution~~ of primary organic aerosols in ~~non-different~~ hygroscopic ~~or hygroscopic~~  
34 ~~mode modes~~. Using the method, we obtain that the ambient internally mixed BC,  
35 accounting for  $80 \pm 20\%$  of total BC aerosol particles, ~~is was~~ retrieved with a campaign  
36 mean density of  $1.1 \pm 0.6 \text{ g cm}^{-3}$  during the observed periods. The retrieved result ~~is was~~  
37 comparable with that reported in the ~~Literature literature~~. By applying a lower ( $0.14 \text{ g}$   
38  $\text{cm}^{-3}$ ) and upper ( $2.1 \text{ g cm}^{-3}$ ) limit of the retrieved BC density in cloud condensation  
39 nuclei (CCN) number ~~concentrations concentration~~ ( $N_{\text{CCN}}$ ) estimation, we derived that  
40 neglect of such variations in BC density would lead to an uncertainty of  $-28\% \sim 11\%$   
41 in predicting  $N_{\text{CCN}}$  at supersaturations of  $0.23\%$  and  $0.40\%$ . We also find that the  $N_{\text{CCN}}$   
42 ~~is was~~ more sensitive to the variations of BC density when it ~~is was~~  $< 1.0 \text{ g cm}^{-3}$ . This  
43 illustrates a necessity of accounting for the effect of BC density on CCN activity closer  
44 to source regions where the BC particles are mostly freshly emitted. The CCN closure  
45 ~~achieves achieved~~ when introducing the retrieved real-time BC density and mixing state.

46 This study provides a unique way of utilizing field measurements to infer ambient BC  
47 density and highlights the importance of applying variable BC density values in models  
48 when predicting CCN and assessing its relevant climate effect.

## 49 **1 Introduction**

50 Black carbon (BC) aerosols, as the major absorber of solar radiation, play a vital  
51 role in energy budget and climate of the earth-atmosphere system by affecting the  
52 radiative forcing and cloud properties (Flanner et al., 2007; Ramanathan and  
53 Carmichael, 2008). The light-absorbing capability induced by BC is related to its  
54 density and morphology (Zhang et al., 2008; Rissler et al., 2014), which can be  
55 modified after mixing with other atmospheric aerosol particles (Khalizov et al., 2009;  
56 Xue et al., 2009). Changes in its physicochemical properties or the aging process would  
57 also regulate its ability to serve as cloud condensation nuclei (CCN) and further  
58 indirectly affect the CCN number concentrations (Zhang et al., 2016a, 2017; Ren et al.,  
59 2023) and the radiative balance by affecting the clouds process (Yuan et al., 2008; Wang  
60 et al., 2011). Owing to the complex evolution of the mixing state, density and  
61 morphology of BC, the contribution of BC particles to CCN budgets is still not well  
62 understood.

63 BC particles, with diesel vehicles, industrial and residential coal combustion as  
64 major sources, are ubiquitous in urban environments (Bond et al., 2013; Dameto et al.,  
65 2017; Li et al., 2017; Liu et al., 2019a). The mixing state of BC describes the  
66 distribution of the bare BC and coating masteries among the aerosol population.

67 Typically, freshly generated BC exists in the form of chain aggregates and initially  
68 uncoated, which is known as externally mixed BC (Ex-BC). When the BC particles  
69 were emitted, they generally mix with other materials by condensation, coagulation,  
70 and other processes (Riemer et al., 2004; Zhang et al., 2008; Liu et al., 2013; Zhang et  
71 al., 2020a), forming the internally mixed BC (In-BC) particles consisting of BC core  
72 and other chemical components (Cheng et al., 2006; Zhang et al., ~~2016~~2016b). The BC  
73 structure would be more compact with regular shapes (Pagels et al., 2009; Zhang et al.,  
74 2008; Wang et al., 2017), and the effective density of internally mixed BC ~~are~~is changed  
75 accordingly with the reconstruction (Liu et al., 2019b). The density and morphology of  
76 BC particles are closely related to its sources, mobility size, coating thickness, coating  
77 material and its chemical composition (~~Zhang et al., 2008;~~ Pagels et al., 2009; ~~Peng et~~  
78 ~~al., 2016;~~ Zhang et al., 2022). A wide range of BC density has been reported in previous  
79 studies (Lide 1992; McMurry et al., 2002; Park et al., 2004; Kiselev et al., 2010). Recent  
80 field ~~measurements have~~measurement has indicated that the average BC density is ~1.2  
81 g cm<sup>-3</sup> in the ambient atmosphere (Zhang et al., ~~2016~~2016b). Field measurements have  
82 also indicated that a considerable fraction of externally mixed/uncoated BC exists  
83 (Clarke et al., 2004; Cheng et al., 2012), although a higher proportion of internally  
84 mixed/aged BC particles in the ambient atmosphere were observed (Schwarz et al.,  
85 2008; Massoli et al., 2015; Chen et al., 2020). In climate models, the BC was generally  
86 assumed completely internally mixed and treated to have a void-free spherical structure  
87 and a density value of 1.8 g cm<sup>-3</sup> (Bond et al., 2013). This may lead to bias in estimating  
88 the climate effect driven by BC.

89 Previous study based on a case study ~~show~~has shown that when the aging degree  
90 of ambient particles ~~is~~was low, the BC density ( $\sim 1.8 \text{ g cm}^{-3}$ ) under the spherical  
91 assumption ~~will~~would lead to the overestimation of particle hygroscopicity by 40-50 %  
92 and the overestimation ~~can~~could be explained almost 100 % using the effective density  
93 of fresh BC ( $\sim 0.45 \text{ g cm}^{-3}$ ) (Fan et al. 2020). This indicates the importance of using  
94 reasonable BC density values in the calculation of particle hygroscopicity. In addition,  
95 when estimating the CCN number concentration, a significant bias of  $-35 \% \sim +20 \%$   
96 was found due to the assumption of particle mixing state (Ren et al., 2018). However,  
97 these studies have not yet accounted for such impact of BC density and mixing state on  
98 CCN prediction due to lack of real time measurement data. Moreover, although the BC  
99 accounts for very small mass fractions (5~10 %) in total fine aerosols, according to our  
100 previous field observed results, the BC-containing particles could contribute 60 %-78 %  
101 toward the total number concentration in urban Beijing (Chen et al., 2020). This is  
102 comparable to the other results using SP2 instrument, which measured that the number  
103 fractions of the coated BC-containing aerosols could be as high as about 50-80 % at the  
104 field sites in north China (Liu et al., 2019b; Zhao et al., 2022). Therefore, the effect of  
105 BC density on the uncertainty of CCN prediction should be concerned carefully.

带格式的: 字体颜色: 自动设置

106 The mixing state and the density of BC particles are usually directly measured by  
107 several techniques, such as an integrated system of a volatility tandem differential  
108 mobility analyzer and a single particle soot photometer (VTDMA-SP2) (Zhang et al.,  
109 ~~2016~~2016b), or a differential mobility analyzer with a SP2 (DMA-SP2) (Olfert et al.,  
110 2007; Rissler et al., 2014; Wu et al., 2019), and a differential mobility analyzer–

111 centrifugal particle analyzer–single-particle soot photometer (DMA–CPMA–SP2)  
112 system (Liu et al., 2019b; Yu et al., 2020), etc. However, such techniques or  
113 measurements are not available in many previously conducted field campaigns. In this  
114 study, we develop a novel method for retrieving the mixing state and effective density  
115 of ambient BC particles by combining field measured hygroscopic growth factor and  
116 aerosol chemical composition and Köhler theory (Petters and Kreidenweis, 2007). The  
117 uncertainty of the new retrieval method was evaluated. The retrieved results were also  
118 compared and validated with existing observations. In addition, the effect of BC density  
119 and mixing state on prediction of CCN number concentrations ~~is~~was further evaluated  
120 through a sensitivity and closure test by accounting for the retrieved real-time variations  
121 of BC density and mixing state.

## 122 **2 Field measurements and methodology**

### 123 **2.1 Field measurements**

124 Measurements in this study were conducted from 15 November to 14 December  
125 2016 at a typical urban site of Beijing (39.97°N, 116.37°E, 49 m above sea level). The  
126 site locates at the Institute of Atmospheric Physics, Chinese Academy of Sciences,  
127 which is mainly influenced by the surrounding cooking, road traffic and residential coal  
128 burning emissions during the home heating periods (Sun et al., 2016). The detailed  
129 information about the sampling site was presented in previous studies (Sun et al.,  
130 ~~2015~~2016; Zhang et al., 2019). The number concentration of condensation nuclei (CN)  
131 at each size was measured by a scanning mobility particle sizer, which ~~is~~was equipped

132 with a differential mobility analyzer (DMA; model 3081, TSI) and a condensation  
133 particle counter (CPC; model 3772, TSI). Subsequently, the mono-dispersed particles  
134 were introduced into a Droplet Measurement Technologies CCN counter (CCNc, DMT;  
135 Lance et al., 2006) to measure CCN number concentration. A hygroscopic tandem  
136 differential mobility analyzer (HTDMA) system was used to measure the hygroscopic  
137 growth factor (Gf) (Tan ~~eret~~ al., 2013). Here, four diameters of 40, 80, 110, 150, and  
138 200 nm ~~are~~were selected in the campaign. Gf is defined as the ratio of the mobility  
139 diameter at the given RH to the dry diameter (Petters and Kreidenweis, 2007). The  
140 nonrefractory submicron aerosol chemical composition was measured by an Aerodyne  
141 high-resolution time-of-flight aerosol mass spectrometer (HR-AMS; Xu et al., 2019),  
142 including sulfate, nitrate, ammonium, chloride, and organics. Two factors, including a  
143 non-hygroscopic primary organic aerosol (POA) and hygroscopic secondary organic  
144 aerosol (SOA) were classified by positive matrix factorization (PMF) with PMF  
145 algorithm (v4.2) method (Paatero and Tapper, 1994) and followed the procedures  
146 reported in Ulbrich et al. (2009). The refractory black carbon mass loading was  
147 measured by an aethalometer (model AE33, Magee Scientific Corporation). Both the  
148 nonrefractory materials and BC mass concentration were measured with diameters <  
149 1.0  $\mu\text{m}$ . The detailed description of the instrument operation and data process have been  
150 described in details elsewhere (Ren et al., 2018; Xu et al., 2019; Zhang et al., 2019; Fan  
151 et al., 2020).

## 152 2.2 Retrieving the mixing state and density of BC

### 153 2.2.1 Retrieving the mixing state of BC

154 The Gf probability distribution function (Gf-PDF) for a specified diameter can be  
155 retrieved firstly based on the TDMAinv algorithm (Gysel et al., 2009). The  $\kappa$ -PDF can  
156 be further calculated based on the Gf-PDF (Fan et al., 2020). Size-resolved  $\kappa$  is derived  
157 using  $\kappa$ -Köhler theory based on hygroscopic growth factor (Gf) (Petters and  
158 Kreidenweis, 2007),

$$159 \quad \kappa_{gf} = (Gf^3 - 1) \cdot \left[ \frac{1}{RH} \exp\left(\frac{4\sigma_{s/a}M_w}{RT\rho_w D_d Gf}\right) - 1 \right] \quad (1)$$

160 where Gf is hygroscopic growth factor, RH is the relative humidity in the HTDMA  
161 (90 %),  $D_d$  is the dry diameter,  $\sigma_{s/a}$  is assumed to be the surface tension of pure water,  
162  $R$  is the universal gas constant,  $T$  is the temperature,  $M_w$  and  $\rho_w$  is the molecular mass,  
163 and the density of water, respectively.

164 The  $\kappa$ -PDF patterns of particles in different sizes always present two modes: nearly  
165 hydrophobic (NH) mode with  $\kappa_{gf} \leq 0.1$  and more hygroscopic (MH) mode with  $\kappa_{gf} >$   
166  $0.1$  (Fig. S1). Firstly, based on the  $\kappa$ -PDF patterns, the number fraction (NF) of the total  
167 nearly hydrophobic group with the boundary of  $[0, 0.1]$  was calculated according to the  
168 following equation:

$$169 \quad NF = \int_0^{0.1} c(\kappa, D_p) d\kappa \quad (2)$$

170 here, the  $\kappa$ -PDF, represented by  $c(\kappa, D_p)$ , was normalized as  $\int c(\kappa, D_p) d\kappa = 1$ , where  
171  $\kappa$  can be replaced by  $\kappa_{gf}$ ,  $D_p$  is the selected electrical mobility diameter in the campaign.

172 The nearly hydrophobic mode consists of both externally mixed POA (Ex-POA or



173 bare POA) and externally mixed BC (Ex-BC). Since the number fraction of the nearly-  
 174 hydrophobic POA would change with the emission and aging processes, in this study,  
 175 we have applied different values for the number fractions of hydrophobic POA (NH-  
 176 POA) under clean (91 %), moderately polluted (70 %), and heavily polluted conditions  
 177 (31 %) by referring to the literature (Liu et al., 2021a), as shown in Fig. S2. The number  
 178 concentration of Ex-BC was then calculated using the total number fraction of NH  
 179 mode minus the number of NH-POA.

$$N_{POA-containing} = N_{total} \times NF_{POA-containing}$$

$$N_{bare-POA} = N_{POA-containing} \times NF_{bare-POA}$$

$$N_{Ex-BC} = N_{NH} - N_{bare-POA} \quad (3)$$

183 where  $N_{POA-containing}$  and  $NF_{POA-containing}$  are the number concentration and fraction of  
 184 POA-containing particles,  $N_{total}$  is the total number concentration,  $N_{bare-POA}$  and  $NF_{bare-}$   
 185 POA are the number concentration and fraction of bare POA particles, and  $N_{NH}$  is the  
 186 number of nearly hydrophobic group.

187 The number size distribution of the externally mixed BC ( $n_{Ex-BC}(\log D_p)$ ) can be  
 188 calculated based on the particle number size distribution (PNSD) and the number  
 189 fraction of the hydrophobic mode of BC ( $NF_{Ex-BC}$ ) as follows:

$$n_{Ex-BC}(\log D_p) = NF_{Ex-BC} \times n(\log D_p) \quad (4)$$

191 where  $n(\log D_p)$  is the function of the aerosol number size distribution,  $D_p$  is the  
 192 mobility diameter.

193 By assuming that the particles ~~are~~ were spherical (Rader and McMurry, 1986), the  
 194 mass size distribution of Ex-BC ( $M_{Ex-BC}$ ) was obtained as follows:

$$M_{\text{Ex-BC}}(\log D_p) = \frac{\pi}{6} D_p^3 \rho n_{\text{Ex-BC}}(\log D_p) \quad (5)$$

196 where  $D_p$  is the mobility diameter,  $\rho$  is the effective density of Ex-BC, and  $n_{\text{Ex-BC}}(\log$   
 197  $D_p)$  is the function of the number size distribution of Ex-BC, respectively. By reviewing  
 198 and summarizing the existing results, we show that typical values of density for the  
 199 freshly emitted or externally mixed BC observed in the winter of urban Beijing or North  
 200 China Plain span over 0.14-0.50 g cm<sup>-3</sup>, with a mean of  $\sim 0.40 \pm 0.10$  g cm<sup>-3</sup> (Fig. S3), in  
 201 the size range of 100 to 300 nm, where the mass concentration of externally mixed BC  
 202 mostly concentrated (Geller et al., 2006; Peng et al., 2016, 2017; Wu et al., 2019; Liu  
 203 et al., 2020; Zhao et al., 2022). Therefore, an average  $\rho_{\text{Ex-BC}}$  of 0.4 g cm<sup>-3</sup> was used for  
 204 calculating the mass concentration of externally mixed BC in our study. Uncertainty  
 205 analyses due to the variations of  $\rho_{\text{Ex-BC}}$  were given in section 2.3.

206 The mass size distribution of Ex-BC was fit using the log-normal distribution as  
 207 shown in Fig. S4 (Wu et al., 2017; Liu et al., 2019a; Zhao et al., 2022). Thus, the bulk  
 208 mass concentration of Ex-BC can be calculated from the integration of the mass size  
 209 distribution:

$$m_{\text{Ex-BC}} = \int_{D_{\text{start}}}^{D_{\text{end}}} M_{\text{Ex-BC}}(\log D_p) d \log(D_p) \quad (6)$$

$$m_{\text{In-BC}} = m_{\text{BC}} - m_{\text{Ex-BC}} \quad (7)$$

212 where  $D_{\text{start}}$  and  $D_{\text{end}}$  are the lower and upper size limit,  $M_{\text{Ex-BC}}(\log D_p)$  is the function  
 213 of the Ex-BC mass size distribution. We then obtained the bulk mass concentration of  
 214 internally mixed BC ( $m_{\text{In-BC}}$ ) by subtracting  $m_{\text{Ex-BC}}$  from the bulk BC mass  
 215 concentration measured by AE33 in equation (7). It should be noted that the mass  
 216 concentration of BC obtained from AE33 based on aerosol light absorption may lead

217 some ~~uncertainty~~uncertainties, as has been further addressed in ~~Section~~section 2.3. \_

#### 218 2.2.2 Retrieving the density of BC

219 For retrieval of the density of BC, the principal idea is to use the measured  $\kappa_{\text{gf}}$  to  
220 calculate the density of BC based on the Zdanovskii–Stokes–Robinson (ZSR) mixing  
221 rule (Stokes and Robinson, 1966; Zdanovskii, 1948) with the chemical composition  
222 measured by AMS (Petters & Kreidenweis, 2007). In the retrieval, several aspects are  
223 concerned. First, since the ZSR rule assumes the aerosol particles are internally mixed,  
224 the  $\kappa_{\text{gf}}$  value of the more MH mode ( $\kappa_{\text{gf-MH}}$ ) is thus applied for retrieving the density of  
225 internally mixed BC. Second, since the size distribution of BC number concentration is  
226 usually with peaks between 100 and 200 nm (Liu et al., 2019a; Yu et al., 2020; Zhao et  
227 al., 2022), the  $\kappa_{\text{gf-MH}}$  value of particles in accumulation mode was averaged and applied  
228 for the retrieval. Previous studies showed an independence of  $\kappa_{\text{gf-MH}}$  on particle size  
229 when the  $D_p > 100$  nm during the campaign period (Fan et al., 2020). Therefore, the  
230 average of  $\kappa_{\text{gf-MH}}$  in accumulation mode is reasonable for the determination of the In-  
231 BC density. Third, since only one hydrophobic and/or one hygroscopic mode was  
232 observed by the HTDMA in most cases during the campaign (Fig. S1, S5), the chemical  
233 components of the more hygroscopic (MH) mode at a given diameter should contain  
234 both these hygroscopic non-BC and the coatings on BC-containing particles, which  
235 would be measured by the HR-AMS instrument together. Therefore, by subtracting the  
236 externally mixed POA in non-hygroscopic mode (see section 2.3), the concentration  
237 and mass fraction of each component measured by HR-AMS can represent the overall

带格式的: 字体颜色: 自动设置

238 chemical composition of MH modes, and thus was applied in the ZSR mixing rule for  
 239 the retrieval of the density of internally mixed BC in this study. In addition, because the  
 240 inversion including measurements from HTDMA and HR-AMS, a total mass closure  
 241 of the measured aerosol particles was conducted between the two techniques by  
 242 comparing the mass concentration of PM<sub>1</sub> and the results are well consistent (Fig. S6).  
 243 The density of internally mixed BC (In-BC),  $\rho_{In-BC}$  is then derived from the following  
 244 equations:

$$245 \quad \kappa_{gf-MH} = \kappa_{chem} = \sum_i \varepsilon_i \kappa_i = \frac{v_{inorg}}{v_{total}} \kappa_{inorg} + \frac{v_{SOA}}{v_{total}} \kappa_{SOA} + \frac{v_{In-POA}}{v_{total}} \kappa_{POA} + \frac{v_{In-BC}}{v_{total}} \kappa_{BC} \quad (8)$$

246 where  $\kappa_{gf-MH}$  is the hygroscopic parameter of the more hygroscopic (MH) mode,  $\kappa_{chem}$   
 247 is the hygroscopic parameter of aerosol particles in the mixed composition and can be  
 248 calculated based on chemical volume fractions using a simple rule (Stokes and  
 249 Robinson, 1966; Petters & Kreidenweis, 2007),  $\kappa_i$  is the hygroscopic parameter of each  
 250 pure composition and  $\varepsilon_i$  is the volume fraction of the individual components in the  
 251 internally mixed particle.  $v_{inorg}$ ,  $v_{SOA}$  and  $v_{In-POA}$  are the volume of the inorganic, SOA  
 252 and internally mixed POA species, and can be calculated as follows:  $v_{inorg} = \frac{m_{inorg}}{\rho_{inorg}}$ ,  
 253  $v_{SOA} = \frac{m_{SOA}}{\rho_{SOA}}$ , and  $v_{In-POA} = \frac{m_{In-POA}}{\rho_{POA}}$ .  $v_{total}$  is the total volume of all the species and can be  
 254 written as  $v_{total} = \frac{m_{inorg}}{\rho_{inorg}} + \frac{m_{SOA}}{\rho_{SOA}} + \frac{m_{In-POA}}{\rho_{POA}} + \frac{m_{In-BC}}{\rho_{In-BC}}$ . In equation (8),  $\kappa_{BC}$  and  $\kappa_{POA}$  are  
 255 assumed to be 0. So, the total volume  $v_{total}$  can be further written as  $v_{total} =$   
 256  $\frac{v_{inorg} \kappa_{inorg} + v_{SOA} \kappa_{SOA}}{\kappa_{gf-MH}}$ . The volume of internally mixed  $v_{In-BC}$  can be calculated as follows,

$$257 \quad v_{In-BC} = \frac{v_{inorg} \kappa_{inorg} + v_{SOA} \kappa_{SOA}}{\kappa_{gf-MH}} - v_{inorg} - v_{SOA} - v_{In-POA}$$

$$258 \quad = \frac{\frac{m_{inorg}}{\rho_{inorg}} \kappa_{inorg} + \frac{m_{SOA}}{\rho_{SOA}} \kappa_{SOA}}{\kappa_{gf-MH}} - \frac{m_{inorg}}{\rho_{inorg}} - \frac{m_{SOA}}{\rho_{SOA}} - \frac{m_{In-POA}}{\rho_{POA}} \quad (9)$$

259 Then then, the  $\rho_{In-BC}$  can be calculated based on its mass concentration and volume as

260 follows:

$$261 \quad \rho_{In-BC} = \frac{m_{In-BC}}{\left( \frac{m_{inorg} \kappa_{inorg} + m_{SOA} \kappa_{SOA}}{\rho_{inorg} \kappa_{gf-MH} + \rho_{SOA}} \frac{m_{inorg} \quad m_{SOA} \quad m_{In-POA}}{\rho_{inorg} \quad \rho_{SOA} \quad \rho_{POA}} \right)} \quad (10)$$

262 where,  $m_{In-BC}$  is the mass concentration of internally mixed BC,  $m_{inorg}$  and  $m_{SOA}$  are the  
 263 mass concentrations of the inorganic species and SOA, which are measured by the AMS.  
 264  $m_{In-POA}$  is the mass concentrations of internally mixed POA and can be calculated  
 265 through subtracting the mass fraction of NH-POA from the total mass concentrations  
 266 of POA.  $\rho_{inorg}$ ,  $\rho_{SOA}$  and  $\rho_{POA}$  are the density of the inorganic species, SOA and POA.  
 267 Since the AMS measures the concentrations of the organic and inorganic ions, including  
 268  $SO_4^{2-}$ ,  $NO_3^-$ ,  $NH_4^+$ ,  $Cl^-$ . Here inorganic species were derived by applying a simplified  
 269 ion pairing scheme (Gysel et al., 2007) to convert mass concentrations of ions to the  
 270 inorganic salts as follows:

$$272 \quad n_{NH_4NO_3} = n_{NO_3^-}$$

$$273 \quad n_{NH_4HSO_4} = \min(2n_{SO_4^{2-}} - n_{NH_4^+} + n_{NO_3^-}, n_{NH_4^+} - n_{NO_3^-})$$

$$274 \quad n_{(NH_4)_2SO_4} = \max(n_{NH_4^+} - n_{NO_3^-} - n_{SO_4^{2-}}, 0)$$

$$271 \quad n_{H_2SO_4} = \max(0, n_{SO_4^{2-}} - n_{NH_4^+} + n_{NO_3^-}) \quad (11)$$

275 where  $n$  represents the number of moles, and the mass concentrations were obtained by  
 276 the number of moles times the molar mass of each inorganic salts. Because the value of  
 277 the  $n_{H_2SO_4}$  was zero in this campaign. Three inorganic salts including  $NH_4HSO_4$ ,  
 278  $(NH_4)_2SO_4$ , and  $NH_4NO_3$  were applied in our study. The densities for inorganic salts  
 279 were taken from previous studies (Gysel et al., 2007; Wu et al., 2016). Here the densities  
 280 for three inorganics are 1.78, 1.77 and 1.72 g cm<sup>-3</sup>, respectively. By summarizing the  
 281 previous studies (Gysel et al., 2007; Dinar et al., 2006), 1.4 g cm<sup>-3</sup> was selected as the

282 density of SOA ( $\rho_{\text{SOA}}$ ). The density of POA ( $\rho_{\text{POA}}$ ) is assumed to be  $1.0 \text{ g cm}^{-3}$  for urban  
283 environments, which is similar to the that of the lubricating oil (Wu et al., 2016). Since  
284 the cooking organic aerosols represent a high contribution to POA in urban  
285 environments, we choose the mean density of the rapeseed oil and oleic acid ( $\sim 0.85 \text{ g}$   
286  $\text{cm}^{-3}$ ) (Reyes-Villegas et al., 2018) to evaluated the result as shown in section 2.3. The  
287 values of  $\kappa$  for inorganic components are 0.56 for  $\text{NH}_4\text{HSO}_4$ , 0.48 for  $(\text{NH}_4)_2\text{SO}_4$  and  
288 0.58 for  $\text{NH}_4\text{NO}_3$ , along with the best-fit values for the three inorganic salts (Petters &  
289 Kreidenweis, 2007 and Gunthe et al., 2009). The  $\kappa_{\text{SOA}}$  is assumed to be 0.15 according  
290 to the field studies in urban areas (Chang et al., 2010; Kawana et al., 2016).

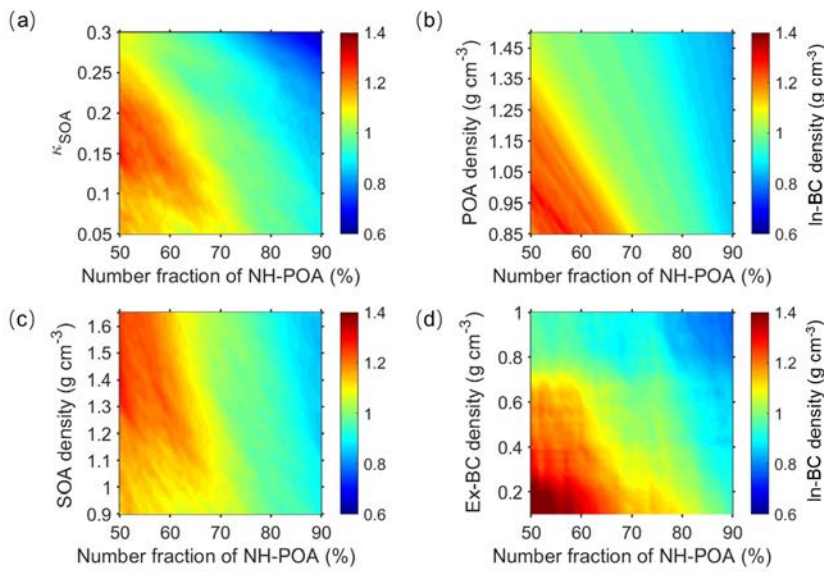
291 Note that the method fails to retrieve the BC density when organic accounts for a  
292 large fraction ( $>60\%$ ). This is because that a higher fraction of OA usually corresponds  
293 to lower total volume of all the species (Fig. S7), yielding negative values for  $v_{\text{In-BC}}$   
294 introduced in equation (9). As a result, 61 % of the data observed during the campaign  
295 were valid for calculating the BC density.

296 Similarly, the bulk density of BC ( $\rho_{\text{bulk-BC}}$ ) is calculated with the same method as  
297 that for calculating the  $\rho_{\text{In-BC}}$ . When calculating the  $\rho_{\text{bulk-BC}}$ , the bulk  $\kappa_{\text{gf}}$  value measured  
298 by HTDMA is applied assuming that all the aerosol particles are internally mixed.

### 299 **2.3 Uncertainties and limitations**

300 For the retrieval, the assumptions on the values of  $\kappa_{\text{SOA}}$ ,  $\rho_{\text{POA}}$ ,  $\rho_{\text{SOA}}$  and  $\rho_{\text{Ex-BC}}$  as  
301 well as the fraction of primary organic aerosols in non-hygroscopic ~~or hygroscopic~~  
302 mode would add uncertainty in the inferred values of ambient internally mixed BC

303 density. For example, the freshly emitted POA particles might consistently be coated  
 304 with the secondary particles during the aging process, resulting in changes of the  $NF_{NH}$ -  
 305 POA. However, a real-time variation of the  $NF_{NH-POA}$  is not yet available due to the lack  
 306 of such ~~measurements data. Applying only the rough fractions of hydrophobic POA for~~



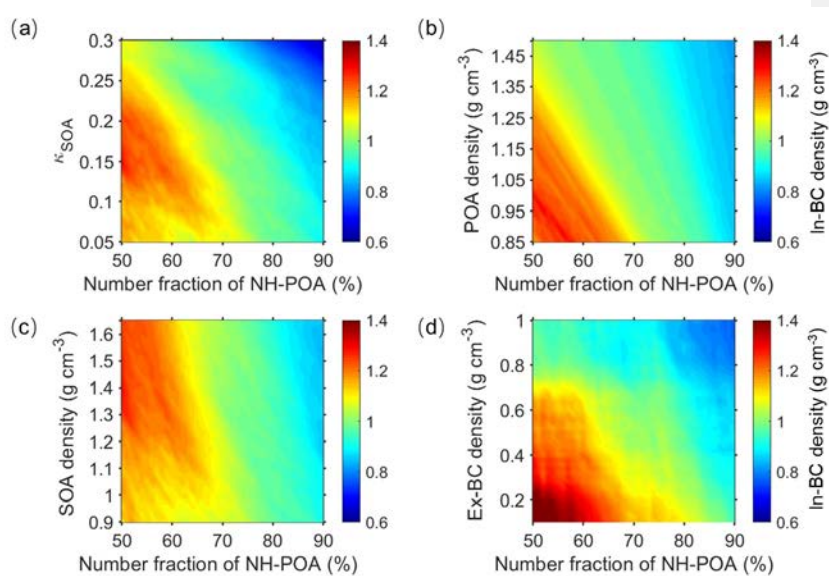
307 ~~measurement data. Applying only rough fractions of hydrophobic POA for~~  
 308 ~~Figure 1. Sensitivities of In-BC density to the variations in the number fraction of nearly hydrophobic (NH) POA~~  
 309 ~~and hygroscopic parameter of OA ( $k_{SOA}$ ) (a), POA density (b), SOA density (c) and the~~  
 310 ~~externally mixed BC density (d).~~

313 three different atmospheric conditions could still cause uncertainties. Also, the  
 314 densities of POA and SOA may differ due to their precursors, emission sources and the  
 315 formation mechanisms in ambient atmosphere (Alfarra et al., 2006; Reyes-Villegas et  
 316 al., 2018). ~~And the~~The density of Ex-BC is generally characterized by the morphology

带格式的

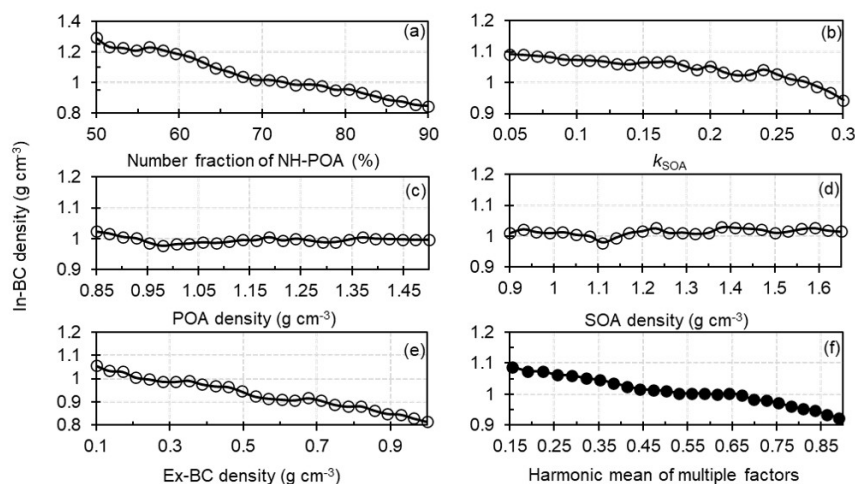
带格式的: 缩进: 首行缩进: 2 字符

317 and size (Wu et al., 2019). In addition, the value of  $\kappa_{\text{SOA}}$  spans largely due to the  
318 variability variations in the emissions of gas precursors and formation processes under  
319 different atmospheric conditions (Zhang et al., 2015; Liu et al., 2021b). Therefore, we  
320 examined the sensitivities of In-BC density to the variations of these factors, as  
321 exhibited in Fig. 1 and Fig. 2.



322  
323 **Figure 1.** Sensitivities of In-BC density to the variations in the number fraction of  
324 nearly hydrophobic (NH) POA and hygroscopic parameter of OA ( $\kappa_{\text{SOA}}$ ) (a), POA  
325 density (b), SOA density (c) and the externally mixed BC density (d).



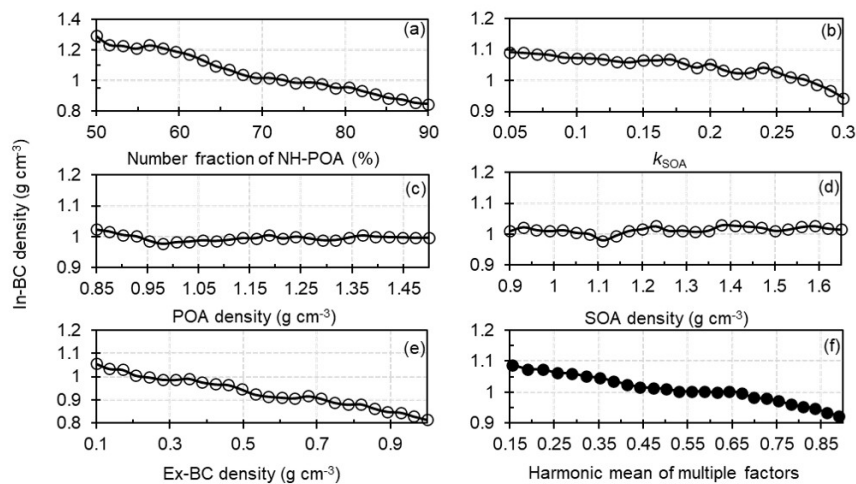


326  
327 **Figure 2.** Sensitivity of the In-BC density to variations in the number fraction of nearly  
328 hydrophobic (NH) POA (a), the hygroscopic parameter of SOA (b), the POA density  
329 (c), the SOA density (d), the externally mixed BC density (e) and the harmonic mean  
330 of multiple factors (f).

331 The figures show that the In-BC density gradually ~~decreases~~decreased with the  
332 increment of the  $NF_{NH-POA}$ , implying the high fraction of bare POA particles  
333 ~~correspond~~corresponded to the early aging stage of aerosol particles. With the increase  
334 of  $\kappa_{SOA}$ , the In-BC density ~~is~~was generally reduced, but with small fluctuations (Fig. 1a,  
335 Fig. 2b). This suggests a complex impact of assumptions of  $\kappa_{SOA}$  on the retrieved BC  
336 density. In addition, the In-BC density ~~decreases~~decreased slightly as  $\rho_{Ex-BC}$   
337 ~~increases~~increased (Fig. 2e), suggesting applying a larger  $\rho_{Ex-BC}$  would derive smaller  
338 values for In-BC density. The In-BC density ~~is~~was insensitive to the changes of the  
339 density of POA and SOA, showing an almost negligible effect on the retrieved results  
340 (Fig. 2c and d).

带格式的: 缩进: 首行缩进: 2 字符

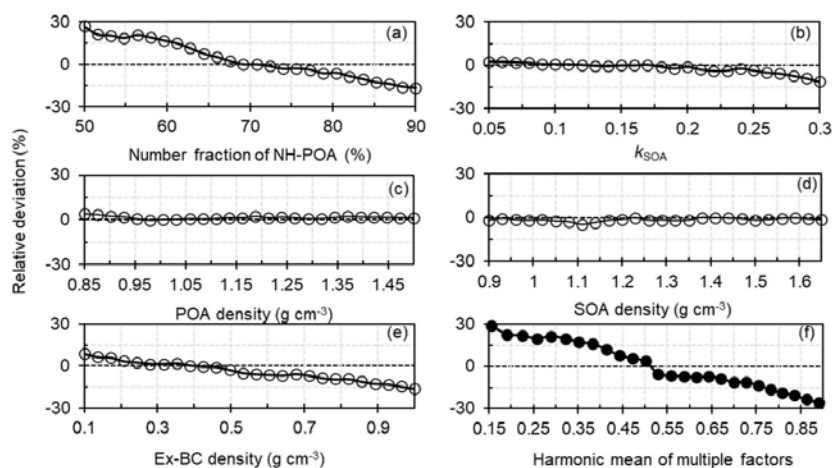
带格式的: 字体: Times New Roman, 小四



341

342 **Figure 2.** Sensitivity of the In-BC density to variations in the number fraction of nearly  
 343 hydrophobic (NH) POA (a), the hygroscopic parameter of SOA (b), the POA density  
 344 (c), the SOA density (d), the externally mixed BC density (e) and the harmonic mean  
 345 of multiple factors (f).

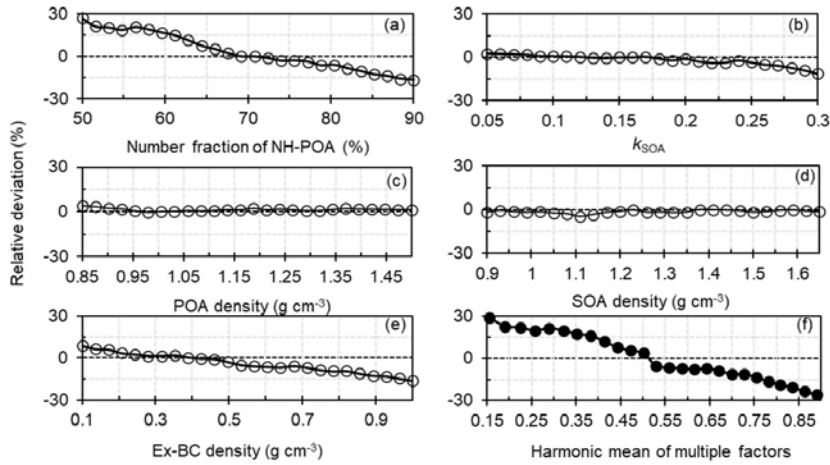
346 The uncertainty analysis shows that, by comparing the results based on the mean  
 347 ~~fractions~~fraction of the  $NF_{NH-POA}$  with a typical atmospheric observed range of 50-90 %  
 348 for the  $NF_{NH-POA}$  (Liu et al., 2021a), ~~we show that~~ the assumption on  $NF_{NH-POA}$  can lead  
 349 to relative deviations (uncertainty) of -17 % ~ +27 % for the retrieved BC density (Fig.  
 350 3a).



351  
352 ~~Figure 3. Relative deviations of the number fraction of nearly hydrophobic (NH) POA~~  
353 ~~to the In-BC density (a), the hygroscopic parameter of OA to the In-BC density (b), the~~  
354 ~~POA density to the In-BC density (c), the SOA density to the In-BC density (d), the~~  
355 ~~externally mixed BC density to In-BC density (e) and the combined deviations based~~  
356 ~~on multiple factors mentioned above (f).~~

357 In addition, unlike inorganics (eg.,  $\text{NH}_4\text{HSO}_4$ ,  $(\text{NH}_4)_2\text{SO}_4$  and  $\text{NH}_4\text{NO}_3$ ), for which  
358 the hygroscopicity has been already well-understood (Petters and Kreidenweis, 2007),  
359 the hygroscopicity of organic species varies largely due to the complexity in organic  
360 aerosol constituents. Therefore, the assumption of the values of  $\kappa_{\text{SOA}}$  will add the  
361 uncertainty in the calculation of BC density. Previous studies have suggested that the  
362 organics hashave a wide range of  $\kappa$  values ranging from 0.05 to 0.3 (Jimenez et al., 2009;  
363 Mei et al., 2013). Thus, the sensitivity test has also been done to examine the effect due  
364 to changes in  $\kappa_{\text{SOA}}$  on calculating the density of BC (Fig. 1a). The result shows that the  
365 assumption of  $\kappa_{\text{SOA}}$  value values can cause an average relative deviation of -10 % ~ +3 %

366 in calculating the density of In-BC (Fig. 3b).



367

368 **Figure 3.** Relative deviations of the number fraction of nearly hydrophobic (NH) POA  
369 to the In-BC density (a), the hygroscopic parameter of OA to the In-BC density (b), the  
370 POA density to the In-BC density (c), the SOA density to the In-BC density (d), the  
371 externally mixed BC density to In-BC density (e) and the combined deviations based  
372 on multiple factors mentioned above (f).

373 However, the sensitivity test shows that the impact of both the  $\rho_{POA}$  and  $\rho_{SOA}$   
374 variations on the BC density estimation ~~is~~ was very small or even negligible (Fig. 1b, c).  
375 By varying the  $\rho_{POA}$  from 0.85 to 1.5  $g\ cm^{-3}$  and the  $\rho_{SOA}$  from 0.9 to 1.65  $g\ cm^{-3}$   
376 according to the ~~literatures~~ literature (Noureddini et al., 1992; Alfarra et al., 2006;  
377 Reyes-Villegas et al., 2018; ~~Cai et al., 2020~~; Kostenidou et al., 2007), the retrieval  
378 uncertainties in the BC density ~~are~~ were both within  $\pm 5\%$  (Fig. 3c, d). For  $\rho_{Ex-BC}$ , it  
379 ~~exhibits~~ exhibited that the evolution of the  $\rho_{Ex-BC}$  could lead to an average deviation of  
380  $-16\% \sim +9\%$  in calculating In-BC density (Fig. 3e) when increasing the values of  $\rho_{Ex-}$

381 bc from 0.1 to 1.0 g cm<sup>-3</sup>, which represents a typical range in ambient atmosphere (Wu  
382 et al., 2019; Liu et al., 2020). A combined uncertainty ( $\delta$ ) caused by the multiple factors  
383 ( $\delta_i$ ), which ~~is~~ was calculated by equation (12, ~~is~~), was -26 % ~ +29 % as shown in Fig.  
384 3f.

$$385 \quad \delta = \sqrt{\sum_{i=1}^n \delta_i^2} \quad (12)$$

386 In addition, it should be noted that the mass concentration of BC obtained from  
387 AE33 based on aerosol light absorption may lead some ~~uncertainty-uncertainties~~.  
388 However, the comparison of the simultaneously measured data by SP2 with ~~that~~ those  
389 by AE33 during the campaign shows that the temporal variations of BC mass  
390 concentrations measured by the two techniques ~~are~~ were well consistent (Fig-~~S5~~, S8).  
391 Note that the BC mass measured by SP2 is occasionally low probably because of the  
392 low detection efficiency in small size (McMeeking et al., 2010; Schwarz et al., 2006).  
393 In addition, the SP2 is unable to quantify the BC mass beyond a certain limit because  
394 of the saturation of electronic devices recording signals (Pileci et al., 2021). We show  
395 that, compared the results that ~~were~~ retrieved if applying the BC mass measured by SP2,  
396 the BC density retrieved based on AE33 can be 18\_% higher. Given ~~that~~ the  
397 measurement bias from SP2, this overestimation indicates an upper limit of the  
398 uncertainty.

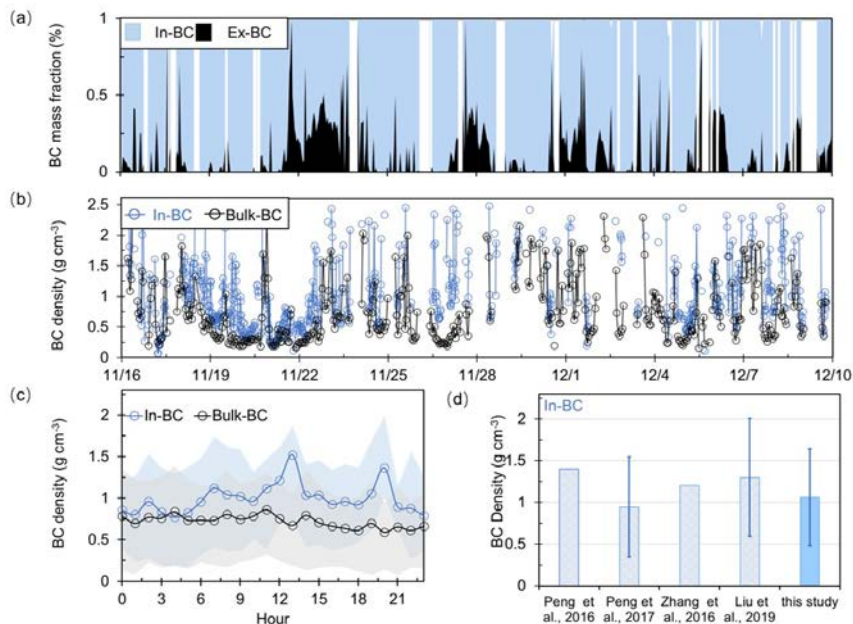
### 399 3 Results and Discussion

#### 400 3.1 ~~Retrieved~~ A comparison and validation of retrieved mixing state and density of 401 ~~BC: comparison and validation\_~~

402 Figure 4a shows retrieved time series of the mixing state of ambient BC during the  
403 campaign. Large temporal variations of the mass fraction of internally and externally  
404 mixed BC ~~are presented~~ present during the observed period at the sites. The temporal  
405 changes should be related to the atmospheric aging process or diurnal variations of  
406 emissions (Liu et al., 2019a; Fan et al., 2020). Statistically, the average mass  
407 ~~fraction~~ fractions of externally and internally mixed BC ~~is/were~~  $20\pm 18\%$  and  $80\pm 20\%$   
408 respectively, showing that most of the BC particles were aged and internally mixed with  
409 other components. Previous studies at urban sites have shown ~~that~~ the co-existence of  
410 the externally mixed BC in the ambient atmosphere (Schwarz et al., 2008; Cheng et al.,  
411 2012; Chen et al., 2020) due to continuous combustion processes (e.g., vehicle exhaust  
412 and residential sector) (Wang et al., 2017; Liu et al., 2019a). Our results are basically  
413 comparable with those

带格式的: 字体颜色: 自动设置

带格式的: 字体颜色: 自动设置



414

415 **Figure 4.** (a) Time series of the mass fraction of the retrieved internal and external  
 416 mixed BC; (b) Time series of the retrieved density of the bulk and internal mixed BC  
 417 (In-BC); (c) Diurnal variation of the retrieved density of bulk and In BC; (d)  
 418 Comparison of the results of the derived In-BC density in this study with that reported  
 419 in literatures.

420 previously reported results, which are directly measured or indirectly retrieved.

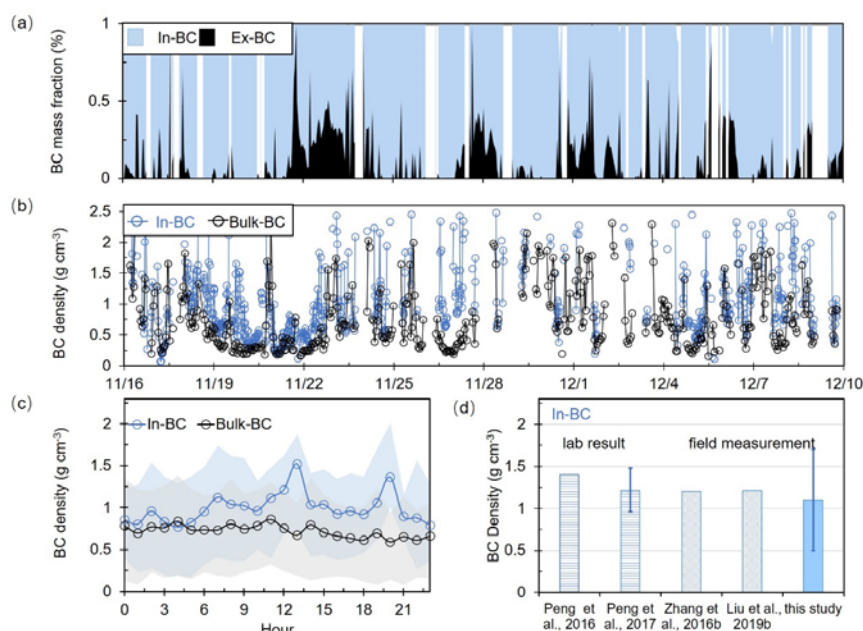
421 For example, Chen et al., (2020) found that the mass fraction of internally mixed BC  
 422 particles was nearly ~80–90 % in summer of Beijing based on VTDMA measurements.

423 Liu et al. (2020), using a tandem system with an aerodynamic aerosol classifier and  
 424 SP2, reported that the mass fraction of internally BC-containing particles would

425 increase with increasing size and reach ~70 % in Beijing. Overall, the mass fraction

426 obtained in our study is was comparable with those that reported in urban Beijing.

427 Previous studies also displayed that the significant diversity of the BC mixing state  
 428 among emission conditions and coating processes (Shiraiwa et al., 2008; Pan et  
 429 al., 2017; Zhang et al., 2020b). Accordingly, the densities of the bulk and internally  
 430 mixed BC present apparent fluctuations as shown in Fig. 4b, which is significantly  
 431 affected by the variations of BC emission sources and its rapid aging  
 432 processes. The density of the In-BC during daytime was

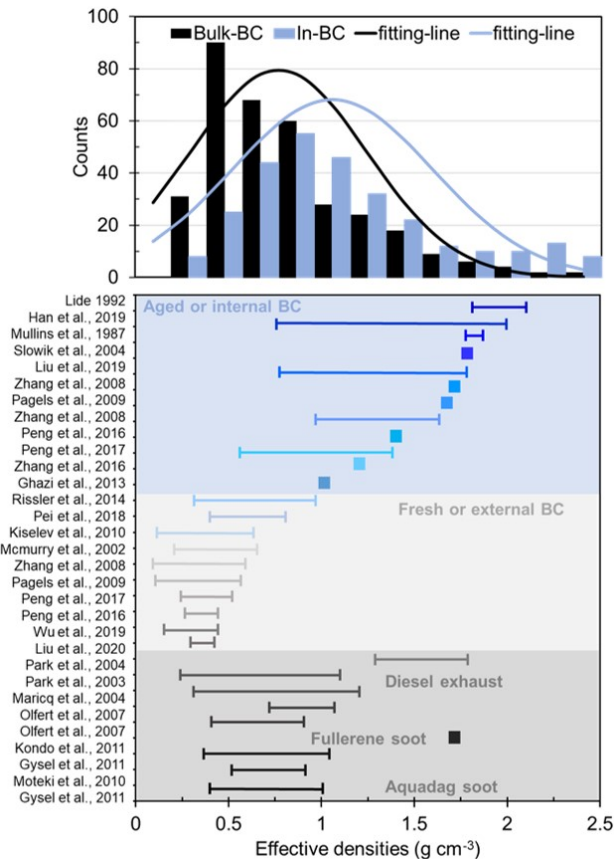


433  
 434 **Figure 4.** (a) Time series of the mass fraction of the retrieved internal- and external-  
 435 mixed BC; (b) Time series of the retrieved density of the bulk and internal- mixed BC  
 436 (In-BC); (c) Diurnal variation of the retrieved density of bulk and In-BC; (d)  
 437 Comparison of the results of the derived In-BC density in this study with that reported  
 438 in the literature.

439 generally higher than that at night (Fig. 4c). The elevated BC density during daytime



440 ~~iswas~~ likely due to ~~that~~ the strong photochemical processes promote the aging of BC  
441 particles, which resulted in a conversion from uncompact structure to compact and  
442 regular spherical shapes of BC (Qiao et al., 2018; Liu et al., 2019b; ~~Zhou et al., 2022~~).  
443 The ~~ffrising~~ in BC density around 20:00 LT might indicate that the BC particles would  
444 be rapidly coated with ~~the~~ secondary inorganic aerosol (SIA) particles and continuously  
445 aged in the polluted period due to the heterogeneous reactions of SIA in urban regions  
446 (Zhang et al., ~~2016~~2016b; Peng et al., 2017). Actually, following the haze evolution, the  
447 fraction of nearly hydrophobic group reduced rapidly (Fig. ~~S8S9~~). Consequently, the  
448 average density of In-BC increased obviously from the clean conditions to the polluted  
449 periods (Fig. ~~S9S5~~). A slight decrease was observed in the bulk BC density during  
450 traffic hours. This is likely associated with the ~~continues~~continuous emissions (e.g.,  
451 vehicle exhaust) that lead to uncoated or uncompact BC particles in this period. The  
452 diurnal cycle in In-BC density ~~iswas~~ consistent with the coating thickness measured by  
453 a tandem CPMA-SP2-DMA-SP2 (Liu et al., 2020), demonstrating that the new method  
454 can derive the density of ambient BC particles reasonably. Averagely, the ~~campaign~~  
455 ~~average values of the~~ bulk and internally mixed BC densities ~~are with campaign~~  
456 ~~averaged values of were~~  $0.7 \pm 0.5$  and  $1.1 \pm 0.6$  g cm<sup>-3</sup> respectively, which ~~are were~~ much  
457 less than 1.8 g cm<sup>-3</sup>, implying that the BC particles ~~isare~~ not ~~a~~-void-free spheres in the  
458 urban atmosphere. The results of In-BC density ~~are were~~ comparable with ~~that~~those  
459 observed at ~~the~~ other sites in North China Plain (NCP) as shown in Fig. 4d, illustrating  
460 that the BC effective density retrieved by this method ~~iswas~~ within the range of ~~density~~  
461 ~~from~~ field measurements. \_\_\_\_



462

463

464

465

466

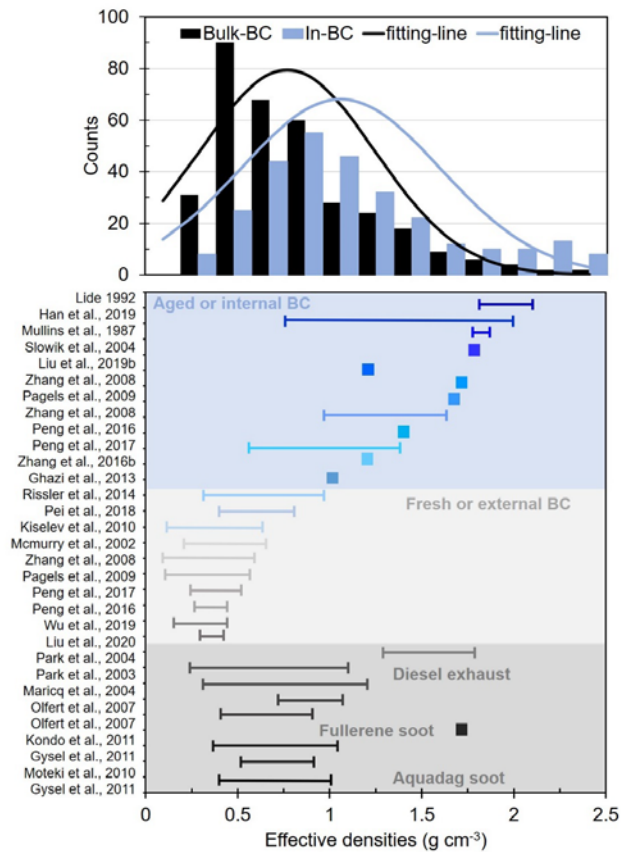
467

468

469

**Figure 5.** The probability distribution function (PDF) of the retrieved density of bulk and In-BC and the measured density distribution spectrum of BC from different sources reported in literatures.

Based on both field measurements (e.g., Lide 1992; Zhang et al., 2016, 2016b; Wu et al., 2019; Liu et al., 2019b) and laboratory studies (e.g., McMurry et al., 2002; Park et al., 2003, 2004; Olfert et al., 2007; Kiselev et al., 2010; Gysel et al., 2011, 2012), the BC density from diverse combustion sources or representing different aging degree has



470

471 **Figure 5.** The probability distribution function (PDF) of the retrieved density of bulk  
 472 and In-BC and the measured density distribution spectrum of BC from different sources  
 473 reported in the literature.

474 been obtained and ranges widely from 0.14 to 2.1 g cm<sup>-3</sup>, as ~~has been~~ summarized  
 475 and shown in Fig. 5. Mean probability distribution function (PDF) of the density of bulk  
 476 and In-BC retrieved by this study is also presented in Fig. 5. It shows that the retrieved  
 477 density of bulk BC ~~exhibits~~ exhibited a dominant mode with a peak value ~~of at~~ 0.7 g cm<sup>-3</sup>  
 478 <sup>3</sup>, which ~~is~~ was situated between the typical density range of those externally mixed and

带格式的: 缩进: 首行缩进: 0 字符

479 internally mixed BC measured previously. For the In-BC, the PDF ~~is~~was with a peak  
480 value at  $1.1 \text{ g cm}^{-3}$ , but ~~ranges~~ranged widely from  $\sim 0.5$  to  $2.5 \text{ g cm}^{-3}$ , which  
481 ~~indicates~~indicated various morphologies, different aging degree and compositions of  
482 ambient BC particles due to the complex impact of multiple local sources and aging  
483 processes during the observed period in urban Beijing. Overall, the retrieved values for  
484 In-BC density fall within the range of typical ~~internal~~internally mixed BC reported in  
485 the ~~literatures~~literature, verifying the reliability of our inversion results.

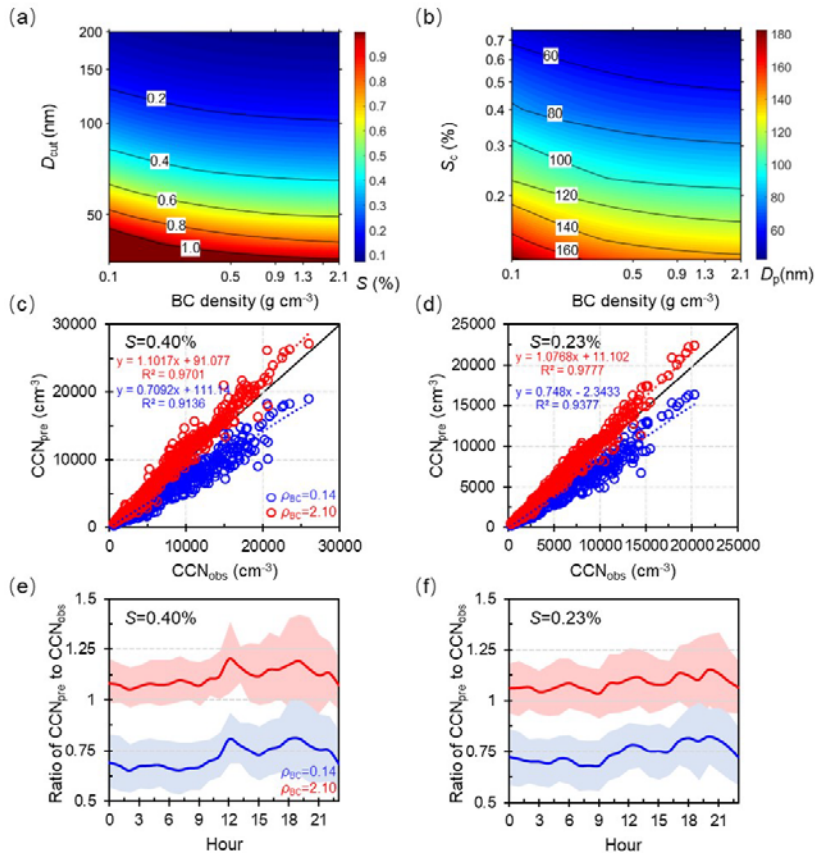
### 486 3.2 Sensitivity of predicted $N_{CCN}$ to changes of BC density

487 A previous study showed that the use of an inaccurate density value of BC particles  
488 would result in large ~~bias~~biases in estimating  $\kappa$  of ambient aerosol particles with the  
489 ZSR mixing rule (Fan et al., 2020), as would further lead to uncertainties in prediction  
490 of  $N_{CCN}$  and relevant climate effects. Considering the large variation range of BC  
491 density

492 during the campaign, which is closely associated with ~~its~~BC morphology or degree  
493 of ~~its~~BC aging, we further examine the sensitivity of critical supersaturation ( $S_c$ ),  
494 critical diameter ( $D_{cut}$ ) and predicted  $N_{CCN}$  to variations of BC density (Fig. 6). Here,  
495 we use the critical diameter and particle number size distribution to calculate  $N_{CCN}$ . ~~The~~  
496 ~~method~~The method to derive the critical diameter is based on Köhler theory and ZSR  
497 rule. Three CCN closure studies were assumed to evaluate the effect of BC density and  
498 mixing state on prediction of CCN number concentrations. Closure studies provide a  
499 useful way to

带格式的: 缩进: 首行缩进: 2 字符

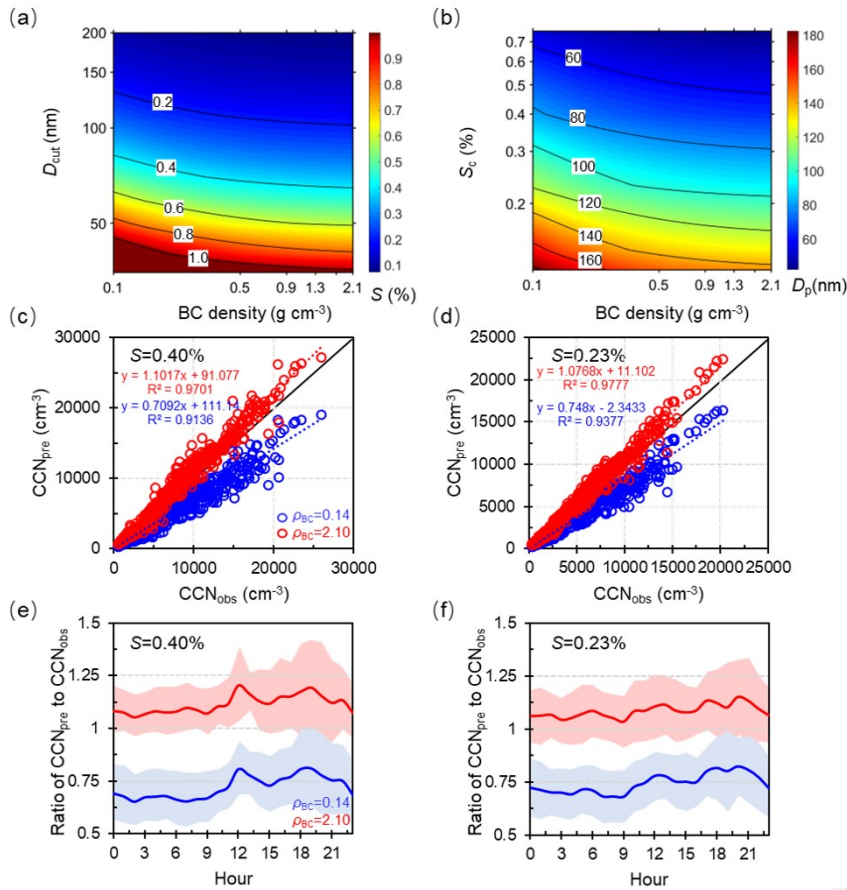
带格式的



500

501

to derive the critical diameter is based on Köhler theory and ZSR rule.



502

503 **Figure 6.** Sensitivity of critical supersaturation ( $S_c$ ) (a) and diameter ( $D_{cut}$ ) (b) to the  
 504 variations in BC density; Predicted  $N_{CCN}$  as a function of measured  $N_{CCN}$  by varying the  
 505 density from 0.14 to 2.1  $\text{g cm}^{-3}$  at  $S=0.40\%$  (c) and  $S=0.23\%$  (d), the black solid line  
 506 is the 1:1 line; Diurnal variations in the ratio of predicted-to-measured  $N_{CCN}$  at  $S=0.40\%$   
 507 (e) and  $S=0.23\%$  (f).

508 investigate the importance of aerosol properties to CCN concentration prediction. If the  
 509 closure study is achieved, it means the bias between the predicted and measured CCN  
 510 concentrations is within  $\pm 15\%$  (Chang et al., 2007). The results show that detailed

带格式的: 缩进: 首行缩进: 0 字符

带格式的

511 ~~calculation methods are presented in the supporting information (SI: Methods) or the~~  
512 ~~reference in Ren et al. (2018). The results show that,~~ by varying the value of density  
513 from 0.14 to 2.1 g cm<sup>-3</sup> that represents the ~~lower and upper limit~~ range of BC density in  
514 the atmosphere, the  $D_{cut}$  ~~reduces~~ reduced apparently at a given supersaturation ( $S$ ) (Fig.  
515 6a), or similarly, the  $S_c$  ~~decreases~~ decreased rapidly for a given particle size (Fig. 6b).  
516 The results show that the changes of the  $D_{cut}$  and  $S_c$  ~~are~~ were more sensitive when the  
517 BC density ~~is~~ was below 1.0 g cm<sup>-3</sup>. ~~And the~~ The effects on the  $D_{cut}$  and  $S_c$  both gradually  
518 weakened with the increase of BC density. This shows that it is critical to apply more  
519 accurate BC density for the aerosol particles with low aging degree in predicting CCN  
520 and its climate effect. Accordingly, the ratios of predicted-to-measured  $N_{CCN}$  ranged  
521 from 0.72 to 1.11 by varying the BC density from 0.14 to 2.1 g cm<sup>-3</sup> at the typical  $S$  of  
522 0.23 % and 0.40 % (Fig. 6c, 6d), showing an estimation uncertainty of -28 % ~ 11 %  
523 in  $N_{CCN}$  prediction.

524 The diurnal variations in the ratio of predicted-to-measured  $N_{CCN}$  at  $S=0.40$  % and  
525 0.23 % are shown to examine the response of the BC density on  $N_{CCN}$  prediction at  
526 different time periods (Fig. 6e, 6f). By applying the lower limit of density value of 0.14  
527 g cm<sup>-3</sup>, the prediction ~~is~~ was much worse ~~compared to~~ than the use of the density of 2.1  
528 g cm<sup>-3</sup> at ~~nighttime~~ night (00:00-06:00 LT), when the latter ~~is~~ was much closer to the real  
529 density of ambient BC (Fig. 4c). The prediction ~~is~~ was improved substantially by  
530 applying the value of 0.14 g cm<sup>-3</sup> during evening rush hours (18:00-20:00 LT), during  
531 which the ambient BC particles ~~is~~ were disturbed by the traffic emissions (Fig. 4c). ~~And~~  
532 ~~now, the~~ The prediction ~~becomes~~ became worse by applying the value of 2.1 g cm<sup>-3</sup>; and

533 an obvious overestimation by up to ~40 % ~~is~~ shown. The results further illustrate  
534 that it is critical to account for the real-time mixing state and density of BC particles in  
535  $N_{CCN}$  prediction, particularly in ~~these~~ regions with heavy traffic and residential coal  
536 emissions.

537 It should be noted that the assumption of the surface tension of water would  
538 overestimate the critical diameter and underpredict CCN number concentration. While  
539 the surface tension depression might be more obvious for the small size particles (<60  
540 nm), as the fraction of organics ~~are~~ is higher at small particles size (Meng et al., 2014;  
541 Cai et al., 2018). Here, in this study, we calculated the critical diameters at  
542 supersaturations of 0.40 % and 0.23 %, typical values in cloud, corresponding to larger  
543 sizes (> 70 nm and 90 nm) of aerosols. Therefore, the uncertainties from the application  
544 of the surface tension of pure water should be negligible (< 10 %). ~~Here, three schemes~~  
545 ~~were assumed to evaluate the effect of BC density and mixing state on prediction of~~  
546 ~~CCN number concentrations. The detailed calculation methods are presented in the~~  
547 ~~supporting information (SI: Methods) or referenced from Ren et al. (2018).~~

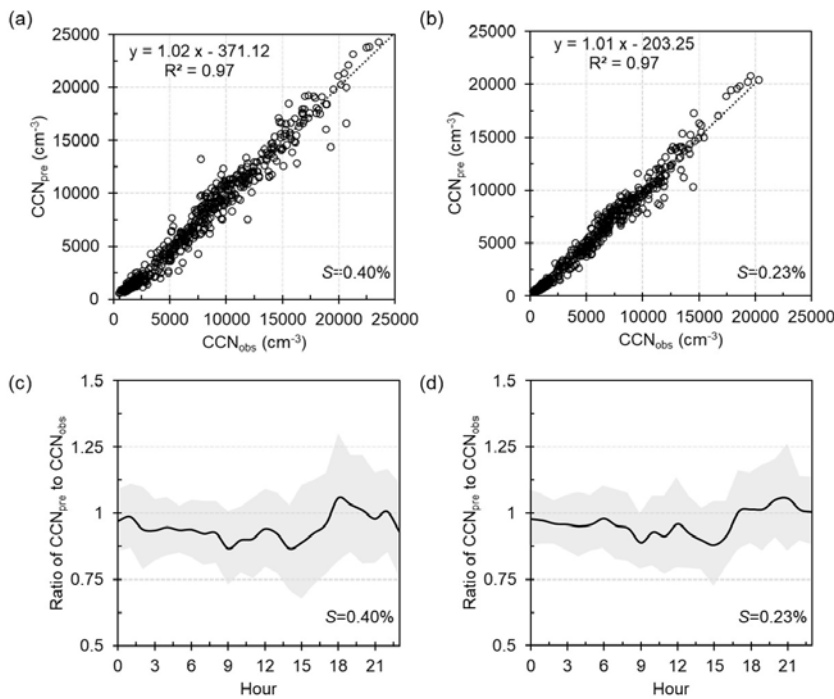
### 548 **3.3 Using $N_{CCN}$ prediction based on the real-time variations of BC density and** 549 **mixing state to predict $N_{CCN}$**

550 Figure 7 exhibits the comparisons between predicted and measured  $N_{CCN}$  at  $S$  of  
551 0.23 % and 0.40 % by accounting for the retrieved real-time variations of BC density  
552 and mixing state. It shows that the  $N_{CCN}$  can be well predicted with a slope of 1.01 and  
553 1.02 at  $S$  of 0.23 % and 0.40 % respectively (Fig. 7a, 7b), only presenting a slight  
554 deviation. The slight deviation is primarily due to the fixed value of the density for the

带格式的: 字体颜色: 自动设置



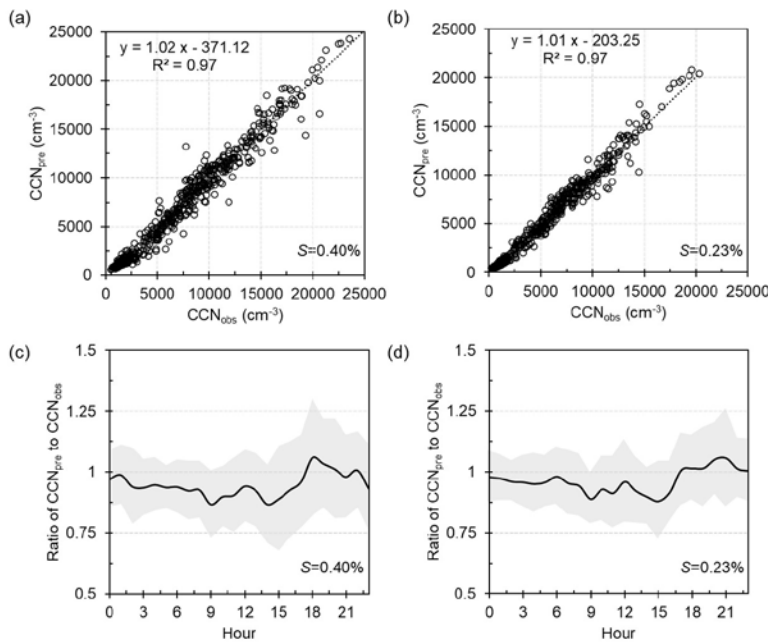
555 externally mixed BC caused by the retrieved method, especially during noontime and  
 556 evening rush periods (Fig. 7c and 7d).



557  
 558 ~~Figure 7. Prediction CCN number concentration using the mixing state and In-BC~~  
 559 ~~density derived from HTDMAs at S=0.40 % (a) and S=0.23 % (b). Diurnal variations~~  
 560 ~~in the ratio of predicted to measured  $N_{CCN}$  at S=0.40 % (c) and S=0.23 % (d).~~

561 The diurnal variations in the ratio of predicted-to-measured  $N_{CCN}$  shows the  $N_{CCN}$   
 562 can be underestimated by up to 15 % at S=0.40 % during ~~these periods: noontime~~. While,  
 563 a slightly overrated during the evening traffic hours and nighttime may be due to the  
 564 underestimation of the number fraction of Ex-BC. Overall, the dependence of the CCN  
 565 prediction on S is due to the size dependence of  $\kappa$  and mixing state (Zhang et al., 2017;  
 566 Liu et al., 2020; ~~XuRen et al., 2021). The 2018~~). A better closure at S=0.23 % is because

567 ~~that~~ the bulk  $\kappa$  of particles is closer to that at the critical diameter ~~corresponding to~~  
 568  ~~$S=0.23\%$ , with  $D_p$~~  of 100-150 nm. Similarly, the effect on CCN prediction induced by  
 569 the bulk mixing state would be more critical for smaller particles, corresponding to the  
 570 critical diameter at high  $S$ .



571  
 572 Figure 7. Predicted CCN number concentration using the mixing state and In-BC  
 573 density derived from HTDMAs at  $S=0.40\%$  (a) and  $S=0.23\%$  (b). Diurnal variations  
 574 in the ratio of predicted-to-measured  $N_{CCN}$  at  $S=0.40\%$  (c) and  $S=0.23\%$  (d).

575 Overall, when considering the effective density of BC relevant to its mixing state,  
 576 the CCN closure achieves. Previous studies have shown that the fresh emitted BC  
 577 particles may convert from fractal-like aggregates to a compact structure and its density  
 578 would increase with the aging process (Pagels et al., 2009; Rissler et al., 2014; Peng et  
 579 al., 2016; Liu et al., 2019b; Zhang et al., 2020a, 2022), but the actual density of In-BC

580 may be lower than  $1.8 \text{ g cm}^{-3}$  in the ambient atmosphere according to this study.  
581 Therefore, the currently applied value represents a density of the void-free structure of  
582 BC particles may cause an overestimation in CCN prediction. In addition, although the  
583 BC accounts for small mass fractions in ambient fine aerosols, according to the  
584 measurements simultaneously conducted at the site, the BC-containing particles could  
585 contribute 60 %-78 % toward the total number concentration in urban Beijing (Chen et  
586 al., 2020). Our results further highlight the effect of BC density on the uncertainty of  
587 CCN prediction should be concerned carefully.

带格式的: 字体颜色: 自动设置

#### 588 4 Conclusions

589 The mixing state and effective density of BC changed through heterogenous  
590 chemistry process and thus would cause uncertainty in evaluating its CCN activity. In  
591 this study, we develop a new method to retrieve the mixing state and effective density  
592 of ambient BC using field measurements and the Köhler theory. The uncertainty of the  
593 new retrieval method was evaluated within  $\pm 30\%$ , which ~~is~~was primarily caused by  
594 assuming the value of  $\kappa_{\text{SOA}}$  and the fraction of primary organic aerosols in non-  
595 hygroscopic mode. The retrieved results show that most of the BC particles were aged  
596 and internally mixed with other components, with mean mass fraction of  $80 \pm 20\%$ .  
597 Averagely, the retrieved densities of the bulk and internally mixed BC ~~are~~were  $0.7 \pm 0.5$   
598 and  $1.1 \pm 0.6 \text{ g cm}^{-3}$  respectively, but ~~range~~ranged widely from  $\sim 0.1$  to  $2.5 \text{ g cm}^{-3}$ ,  
599 indicating various morphologies, different aging degree and compositions of ambient  
600 BC particles due to the complex impact of multiple local sources and aging processes

601 during the observed period. The retrieved ~~results are~~result was basically comparable  
602 with ~~the~~ previous observations in North China Plain.

603 Further examination shows the uncertainties of the  $N_{CCN}$  prediction ~~is with~~  
604 ~~uncertainties of were~~ -28 % ~ 11 % at the typical  $S$  of 0.23 % and 0.40 % by varying the  
605 BC density from 0.14 to 2.1 g cm<sup>-3</sup> that ~~represents~~represented the ~~lower and upper~~  
606 ~~limit range~~ of ambient BC particles. Moreover, the prediction ~~is was~~ found more  
607 sensitive to the ~~variability~~variations of BC density when it ~~is was~~ <1.0 g cm<sup>-3</sup>, suggesting  
608 a great significance ~~to account of~~accounting for the effect of BC density for the aerosol  
609 particles with low aging degree when evaluating the climate effect. The CCN closure  
610 ~~achieves~~achieved when introducing the retrieved real-time BC density relevant to its  
611 mixing state. This work provides a unique way of utilizing field observations to infer  
612 ambient BC density and highlights the current assumption of a void-free structure of  
613 BC particles in models would cause large uncertainties in CCN prediction and in the  
614 relevant climate effect evaluation.

615 The method used to derive the ambient BC density has limitations. Since the  
616 assumptions on the values of  $\kappa_{SOA}$ ,  $\rho_{POA}$ ,  $\rho_{SOA}$  and  $\rho_{Ex-BC}$  as well as the fraction of  
617 primary organic aerosols in non-hygroscopic ~~or hygroscopic~~ mode would add  
618 uncertainty in the inferred values of ambient internally mixed BC density. It is thus  
619 necessary to examine observational data to verify this methodology in ~~further~~future  
620 studies. However, the method and results of this study could provide the way for a more  
621 comprehensive understanding of the ~~variability~~variations in BC density in Beijing.  
622 Additionally, it has the potential to reveal the uncertainties of usage of void-free

带格式的

623 structure of BC density in ~~accessing~~assessing the climate effects.

#### 624 **Data availability.**

625 All data needed to evaluate the conclusions in the paper are present in the paper and/or  
626 the Supplement. All data used in the study are also available from the corresponding  
627 author upon request (zhangfang2021@hit.edu.cn).

#### 628 **Author contributions.**

629 FZ and JR conceived the conceptual development of the manuscript. JR directed and  
630 performed of the experiments with JL, LC, and FZ. JR conducted the data analysis and  
631 wrote the draft of the manuscript. All authors edited and commented on the various  
632 sections of the manuscript.

#### 633 **Acknowledgments.**

634 This work was funded by the National Natural Science Foundation of China (NSFC)  
635 research project (41975174, 41675141), Shenzhen Science and Technology Plan  
636 Project (Grant No. GXWD20220811174022002). We thank all participants in the field  
637 campaigns for their tireless work and cooperation. We also thank Dr. Yele Sun and his  
638 group for providing the data of nonrefractory submicron aerosol chemical composition.

639 **Competing interests.**

640 The contact author has declared that neither they nor their co-authors have any  
641 competing interests.

642 **References**

643 Alfarra, M. R., Paulsen, D., Gysel, M., Garforth, A. A., Dommen, J., Prévôt, A. S. H.,  
644 Worsnop, D. R., Baltensperger, U., and Coe, H.: A mass spectrometric study of  
645 secondary organic aerosols formed from the photooxidation of anthropogenic and  
646 biogenic precursors in a reaction chamber, *Atmos. Chem. Phys.*, 6, 5279– 5293,  
647 <https://doi.org/10.5194/acp-6-5279-2006>, 2006.

648 Bond, T. C., Doherty, S. J., Fahey, D., Forster, P., Berntsen, T., DeAngelo, B., Flanner,  
649 M., Ghan, S., Kärcher, B., and Koch, D.: Bounding the role of black carbon in the  
650 climate system: A scientific assessment, *J. Geophys. Res.-Atmos.*, 118(11), 5380–  
651 5552, <https://doi.org/10.1002/jgrd.50171>, 2013.

652 [Cheng, Y. F., Eichler, H., Wiedensohler, A., Heintzenberg, J., Zhang, Y. H., Hu, M.,](#)  
653 [Herrmann, H., Zeng, L. M., Liu, S., Gnauk, T., Brüggemann, E., and He, L. Y.:](#)  
654 [Mixing state of elemental carbon and non-light-absorbing aerosol components](#)  
655 [derived from in situ particle optical properties at Xinken in Pearl River Delta of China,](#)  
656 [J. Geophys. Res., 111, D20204, doi:10.1029/2005JD006929, 2006.](#)

657 Clarke, A.D., Shinozuka, Y., Kapustin, V.N., Howell, S., Huebert, B., Doherty, S.,  
658 Anderson, T., Covert, D., Anderson, J., Hua, X., Moore II, K.G., McNaughton, C.,  
659 Carmichael, G., Weber, R.: Size distributions and mixtures of dust and black carbon  
660 aerosol in Asian outflow: physiochemistry and optical properties, *J. Geophys. Res.-*  
661 *Atmos.*, 109, D15S09, <https://doi.org/10.1029/2003JD004378>, 2004.

662 Cheng, Y. F., Su, H., Rose, D., Gunthe, S. S., Berghof, M., Wehner, B., Achtert, P.,  
663 Nowak, A., Takegawa, N., Kondo, Y., Shiraiwa, M., Gong, Y. G., Shao, M., Hu, M.,  
664 Zhu, T., Zhang, Y. H., Carmichael, G. R., Wiedensohler, A., Andreae, M. O., and  
665 Pöschl, U.: Size-resolved measurement of the mixing state of soot in the megacity  
666 Beijing, China: diurnal cycle, aging and parameterization, *Atmos. Chem. Phys.*, 12,  
667 4477–4491, <https://doi.org/10.5194/acp-12-4477-2012>, 2012.

668 ~~[Cheng, Y. F., Eichler, H., Wiedensohler, A., Heintzenberg, J., Zhang, Y. H., Hu, M.,](#)~~  
669 ~~[Herrmann, H., Zeng, L. M., Liu, S., Gnauk, T., Brüggemann, E., and He, L. Y.:](#)~~  
670 ~~[Mixing state of elemental carbon and non light absorbing aerosol components](#)~~  
671 ~~[derived from in situ particle optical properties at Xinken in Pearl River Delta of China,](#)~~  
672 ~~[J. Geophys. Res., 111, D20204, doi:10.1029/2005JD006929, 2006.](#)~~

673 Chen, L., F. Zhang, P. Yan, X. Wang, L. Sun, Y. Li, X. Zhang, Y. Sun, and Z. Li.: The  
674 large proportion of black carbon (BC)-containing aerosols in the urban atmosphere,

带格式的: 超链接, 字体: +西文正文 (等线), 五号

675 Environ. Pollut., 263, 114507, <https://doi.org/10.1016/j.envpol.2020.114507>, 2020.  
676 Chang, R. Y.-W., Slowik, J. G., Shantz, N. C., Vlasenko, A., Liggio, J., Sjostedt, S. J.,  
677 Leaitch, W. R., and Abbatt, J. P. D.: The hygroscopicity parameter ( $k$ ) of ambient  
678 organic aerosol at a field site subject to biogenic and anthropogenic influences:  
679 relationship to degree of aerosol oxidation, *Atmos. Chem. Phys.*, 10, 5047–5064,  
680 <https://doi:10.5194/acp-10-5047-2010>, 2010.

681 [Chang, R. Y. W., Liu, P. S. K., Leaitch, W. R., and Abbatt, J. P. D.: Comparison](#)  
682 [between measured and predicted CCN concentrations at Egbert, Ontario: Focus on](#)  
683 [the organic aerosol fraction at a semirural site, \*Atmos. Environ.\*, 41, 8172–8182,](#)  
684 <https://doi:10.1016/j.atmosenv.2007.06.039>, 2007.

带格式的

带格式的

685 Cai, M., Tan, H., Chan, C. K., Qin, Y., Xu, H., Li, F., Schurman, M. I., Liu, L., and Zhao,  
686 J.: The size-resolved cloud condensation nuclei (CCN) activity and its prediction  
687 based on aerosol hygroscopicity and composition in the Pearl Delta River (PRD)  
688 region during wintertime 2014, *Atmos. Chem. Phys.*, 18, 16419–16437,  
689 <https://doi.org/10.5194/acp-18-16419-2018>, 2018.

690 [Cai, J., Chu, B., Yao, L., Yan, C., Heikkinen, L. M., Zheng, F., Li, C., Fan, X., Zhang,](#)  
691 [S., Yang, D., Wang, Y., Kokkonen, T. V., Chan, T., Zhou, Y., Dada, L., Liu, Y., He,](#)  
692 [H., Paasonen, P., Kujansuu, J. T., Petäjä, T., Mohr, C., Kangasluoma, J., Bianchi, F.,](#)  
693 [Sun, Y., Croteau, P.-L., Worsnop, D. R., Kerminen, V. M., Du, W., Kulmala, M., and](#)  
694 [Daellenbach, K. R.: Size segregated particle number and mass concentrations from](#)  
695 [different emission sources in urban Beijing, \*Atmos. Chem. Phys.\*, 20, 12721–12740,](#)  
696 <https://doi.org/10.5194/acp-20-12721-2020>, 2020.

带格式的: 超链接, 字体: +西文正文 (等线), 五号

带格式的

带格式的

带格式的: 超链接, 字体: +西文正文 (等线), 五号

697 [Dinar, E., Mentel, T. F., and Rudich, Y.: The density of humic acids and humic like](#)  
698 [substances \(HULIS\) from fresh and aged wood burning and pollution aerosol](#)  
699 [particles, \*Atmos. Chem. Phys.\*, 6, 5213–5224, doi:10.5194/acp-6-5213-2006, 2006,](#)

带格式的: 超链接, 字体: +西文正文 (等线), 五号

700 Dameto de España, C., Wonauschütz, A., Steiner, G., Rosati, B., Demattio, A., Schuh,  
701 H., and Hitznerberger, R.: Long-term quantitative field study of New Particle  
702 Formation (NPF) events as a source of Cloud Condensation Nuclei (CCN) in the  
703 urban background of Vienna, *Atmos. Environ.*, 164, 289–298,  
704 <https://doi.org/10.1016/j.atmosenv.2017.06.001>, 2017.

带格式的: 下划线

705 [Dinar, E., Mentel, T. F., and Rudich, Y.: The density of humic acids and humic like](#)  
706 [substances \(HULIS\) from fresh and aged wood burning and pollution aerosol](#)  
707 [particles, \*Atmos. Chem. Phys.\*, 6, 5213–5224, doi:10.5194/acp-6-5213-2006, 2006,](#)

带格式的: 超链接, 字体: +西文正文 (等线), 五号

708 Flanner, M. G., Zender, C. S., Randerson, J. T., and Rasch, P. J.: Present-day climate  
709 forcing and response from black carbon in snow, *J. Geophys. Res.-Atmos.*, 112,  
710 D11202, <https://doi.org/10.1029/2006JD008003>, 2007.

711 Fan, X., Liu, J., Zhang, F., Chen, L., Conllins, D., Xu, W., Jin, X., Ren, J., Wang, Y., Wu,  
712 H., Li, S., Sun, Y., Li, Z.: Contrasting size-resolved hygroscopicity of fine particles  
713 derived by HTDMA and HR-ToF-AMS measurements between summer and winter  
714 in Beijing: the impacts of aerosol aging and local emissions, *Atmos. Chem. Phys.* 20,  
715 915–929, <https://doi.org/10.5194/acp-20-915-2020>, 2020.

带格式的: 下划线

716 [Gysel, M., McFiggans, G. B., and Coe, H.: Inversion of tandem differential mobility](#)  
717 [analyser \(TDMA\) measurements, \*J. Aerosol Sci.\*, 40, 134–151,](#)  
718 <https://doi.org/10.1016/j.jaerosci.2008.07.013>, 2009.

带格式的

带格式的: 超链接, 字体: +西文正文 (等线), 五号

719 Geller, M., Biswas, S., and Sioutas, C.: Determination of particle effective density in  
720 urban environments with a differential mobility analyzer and aerosol particle mass  
721 analyzer, *Aerosol Sci. Technol.*, 40, 709–723,  
722 <https://doi.org/10.1080/02786820600803925>, 2006.

723 ~~Gysel, M., McFiggans, G. B., and Coe, H.: Inversion of tandem differential mobility  
724 analyser (TDMA) measurements, *J. Aerosol Sci.*, 40, 134–151,  
725 <https://doi.org/10.1016/j.jaerosci.2008.07.013>, 2009.~~

726 ~~Gysel, M., Crosier, J., Topping, D. O., Whitehead, J. D., Bower, K. N., Cubison, M. J.,  
727 Williams, P. I., Flynn, M. J., McFiggans, G. B., and Coe, H.: Closure study between  
728 chemical composition and hygroscopic growth of aerosol particles during TORCH2,  
729 *Atmos. Chem. Phys.*, 7, 6131–6144, <https://doi.org/10.5194/acp-7-6131-2007>, 2007.~~  
730 Gunthe, S. S., King, S. M., Rose, D., Chen, Q., Roldin, P., Farmer, D. K., Jimenez, J.  
731 L., Artaxo, P., Andreae, M. O., Martin, S. T., and Pöschl, U.: Cloud condensation  
732 nuclei in pristine tropical rainforest air of Amazonia: size resolved measurements and  
733 modeling of atmospheric aerosol composition and CCN activity, *Atmos. Chem. Phys.*,  
734 9, 7551–7575, <https://doi.org/10.5194/acp-9-7551-2009>, 2009.

735 Gysel, M., Laborde, M., Olfert, J. S., Subramanian, R., & Gröhn, A. J.: Effective density  
736 of aquadag and fullerene soot black carbon reference materials used for SP2  
737 calibration, *Atmos. Meas. Tech.*, 4(12), 4937–4955, <https://doi.org/10.5194/amt-4-2851-2011>, 2011.

739 Gysel, M., Laborde, M., Mensah, A. A., Corbin, J. C., Keller, A., Kim, J., et al.:  
740 Technical note: The single particle soot photometer fails to reliably detect PALAS  
741 soot nanoparticles, *Atmos. Meas. Tech.*, 5(12), 3099–3107,  
742 <https://doi.org/10.5194/amt-5-3099-2012>, 2012.

743 Jimenez, J. L., Canagaratna, M. R., Donahue, N. M., Prevot, A. S. H., Zhang, Q., Kroll,  
744 J. H., DeCarlo, P. F., Allan, J. D., Coe, H., Ng, N. L., Aiken, A. C., Docherty, K. S.,  
745 Ulbrich, I. M., Grieshop, A. P., Robinson, A. L., Duplissy, J., Smith, J. D., Wilson,  
746 K. R., Lanz, V. A., Hueglin, C., Sun, Y. L., Tian, J., Laaksonen, A., Raatikainen, T.,  
747 Rautiainen, J., Vaattovaara, P., Ehn, M., Kulmala, M., Tomlinson, J. M., Collins, D.  
748 R., Cubison, M. J., Dunlea, E. J., Huffman, J. A., Onasch, T. B., Alfarra, M. R.,  
749 Williams, P. I., Bower, K., Kondo, Y., Schneider, J., Drewnick, F., Borrmann, S.,  
750 Weimer, S., Demerjian, K., Salcedo, D., Cottrell, L., Griffin, R., Takami, A., Miyoshi,  
751 T., Hatakeyama, S., Shimojo, A., Sun, J. Y., Zhang, Y. M., Dzepina, K., Kimmel, J.  
752 R., Sueper, D., Jayne, J. T., Herndon, S. C., Trimborn, A. M., Williams, L. R., Wood,  
753 E. C., Middlebrook, A. M., Kolb, C. E., Baltensperger, U., and Worsnop, D. R.:  
754 Evolution of Organic Aerosols in the Atmosphere, *Science*, 326, 1525–1529,  
755 <https://doi.org/10.1126/science.1180353>, 2009.

756 –  
757 ~~[Khalizov, A. F., Zhang, R., Zhang, D., Xue, H., Pagels, J., and McMurry, P. H.:  
758 Formation of highly hygroscopic soot aerosols upon internal mixing with sulfuric  
759 acid vapor, \*J. Geophys. Res.-Atmos.\*, 114, D05208,  
760 <https://doi.org/10.1029/2008jd010595>, 2009.](#)~~

761 Kiselev, A., Wennrich, C., Stratmann, F., Wex, H., Henning, S., Mentel, T.F., Kiendler-  
762 Scharr, A., Schneider, J., Walter, S., Lieberwirth, I.: Morphological characterization

带格式的

带格式的: 超链接, 字体: +西文正文(等线), 五号

带格式的



- 763 of soot aerosol particles during LACIS Experiment in November (LEXNo), J.  
764 Geophys. Res. -Atmos., 115, D11204. <https://doi.org/10.1029/2009jd012635>, 2010.
- 765 ~~Khalizov, A. F., Zhang, R., Zhang, D., Xue, H., Pagels, J., and McMurry, P. H.:  
766 Formation of highly hygroscopic soot aerosols upon internal mixing with sulfuric  
767 acid vapor, J. Geophys. Res. Atmos., 114, D05208,  
768 <https://doi.org/10.1029/2008jd010595>, 2009.~~
- 769 Kawana, K., Nakayama, T., and Mochida, M.: Hygroscopicity and CCN activity of  
770 atmospheric aerosol particles and their relation to organics: Characteristics of urban  
771 aerosols in Nagoya, Japan, J. Geophys. Res.-Atmos., 121, 4100–4121,  
772 <https://doi.org/10.1002/2015JD023213>, 2016.
- 773 Kostenidou, E., Pathak, R. K., & Pandis, S. N.: An Algorithm for the Calculation of  
774 Secondary Organic Aerosol Density Combining AMS and SMPS Data, Aerosol  
775 Science and Technology, 41:11, 1002-1010, [https://doi:  
776 10.1080/02786820701666270](https://doi:10.1080/02786820701666270), 2007.
- 777 Li, M., Zhang, Q., Kurokawa, J.-I., Woo, J.-H., He, K., Lu, Z., Ohara, T., Song, Y.,  
778 Streets, D. G., Carmichael, G. R., Cheng, Y., Hong, C., Huo, H., Jiang, X., Kang, S.,  
779 Liu, F., Su, H., and Zheng, B.: MIX: a mosaic Asian anthropogenic emission  
780 inventory under the international collaboration framework of the MICS-Asia and  
781 HTAP, Atmos. Chem. Phys., 17, 935–963, <https://doi.org/10.5194/acp-17-935-2017>,  
782 2017.
- 783 Liu, D., Joshi, R., Wang, J., Yu, C., Allan, J. D., Coe, H., Flynn, M. J., Xie, C., Lee, J.,  
784 Squires, F., Kotthaus, S., Grimmond, S., Ge, X., Sun, Y., and Fu, P.: Contrasting  
785 physical properties of black carbon in urban Beijing between winter and summer,  
786 Atmos. Chem. Phys., 19, 6749–6769, <https://doi.org/10.5194/acp-19-6749-2019>,  
787 2019a.
- 788 Liu, D., Allan, J., Whitehead, J., Young, D., Flynn, M., Coe, H., McFiggans, G.,  
789 Fleming, Z. L., and Bandy, B.: Ambient black carbon particle hygroscopic properties  
790 controlled by mixing state and composition, Atmos. Chem. Phys., 13, 2015–2029,  
791 <https://doi.org/10.5194/acp-13-2015-2013>, 2013.
- 792 Liu, H., Pan, X.L., Wu, Y., Wang, D.W., Tian, Y., Liu, X.Y., et al.: Effective densities of  
793 soot particles and their relationships with the mixing state at an urban site in the  
794 Beijing megacity in the winter of 2018, Atmos. Chem. Phys. 19, 14791–14804,  
795 <https://doi.org/10.5194/acp-19-14791-2019>, 2019b.
- 796 Lide, D. R. (ed.). CRC Handbook of Chemistry and Physics. CRC Press: Ann Arbor,  
797 MI. (1992).
- 798 Lance, S., Medina, J., Smith, J., and Nenes, A.: Mapping the operation of the DMT  
799 continuous flow CCN counter, Aerosol Sci. Tech., 40, 242–254,  
800 <https://doi.org/10.1080/02786820500543290>, 2006.
- 801 ~~Liu, H., Pan, X., Liu, D., Liu, X., Chen, X., Tian, Y., Sun, Y., Fu, P., and Wang, Z.:  
802 Mixing characteristics of refractory black carbon aerosols at an urban site in Beijing,  
803 Atmos. Chem. Phys., 20, 5771–5785, <https://doi.org/10.5194/acp-20-5771-2020>,  
804 2020.~~
- 805 Liu, L., Zhang, J., Zhang, Y., Wang, Y., Xu, L., Yuan, Q., et al.: Persistent residential  
806 burning-related primary organic particles during wintertime hazes in North China:

带格式的: 下划线

带格式的: 超链接, 字体: +西文正文 (等线), 五号

807 insights into their aging and optical changes, *Atmos. Chem. Phys.* *21*, 2251–2265,  
808 <https://doi.org/10.5194/acp-21-2251-2021>, 2021a.

809 [Liu, H., Pan, X., Liu, D., Liu, X., Chen, X., Tian, Y., Sun, Y., Fu, P., and Wang, Z.:  
810 \*Mixing characteristics of refractory black carbon aerosols at an urban site in Beijing\*,  
811 \*Atmos. Chem. Phys.\*, \*20\*, 5771–5785, <https://doi.org/10.5194/acp-20-5771-2020>,  
812 2020.](#)

813 [Liu, J., Zhang, F., Xu, W., Sun, Y., Chen, L., Li, S.: Hygroscopicity of organic aerosols  
814 linked to formation mechanisms, \*Geophysical Research Letters\*, \*48\*, e2020GL091683,  
815 <https://doi.org/10.1029/2020gl091683>, 2021b.](#)

816 McMurry, H. Peter, Wang Xin, Park Kihong & Ehara Kensei.: The Relationship  
817 between Mass and Mobility for Atmospheric Particles: A New Technique for  
818 Measuring Particle Density, *Aerosol Sci. Technol.*, *36*:2, 227-238,  
819 <https://doi.org/10.1080/027868202753504083>, 2002.

820 Massoli, P., Onasch, T.B., Cappa, C.D., Nuamaan, I., Hakala, J., Hayden, K., Li, S.M.,  
821 Sueper, D.T., Bates, T.S., Quinn, P.K., Jayne, J.T., Worsnop, D.R.: Characterization  
822 of black carbon-containing particles from soot particle aerosol mass spectrometer  
823 measurements on the R/V Atlantis during CalNex 2010, *J. Geophys. Res.- Atmos.*,  
824 *120*, 2575-2593, <https://doi.org/10.1002/2014JD022834>, 2015.

825 Mei, F., Setyan, A., Zhang, Q., and Wang, J.: CCN activity of organic aerosols observed  
826 downwind of urban emissions during CARES, *Atmos. Chem. Phys.*, *13*, 12155–  
827 12169, <https://doi.org/10.5194/acp-13-12155-2013>, 2013.

828 ~~[Meng, J. W., Yeung, M. C., Li, Y. J., Lee, B. Y. L., and Chan, C. K.: Size-resolved cloud  
829 condensation nuclei \(CCN\) activity and closure analysis at the HKUST Supersite in  
830 Hong Kong, \*Atmos. Chem. Phys.\*, \*14\*, 10267–10282, \[https://doi.org/10.5194/acp-14-  
831 10267-2014\]\(https://doi.org/10.5194/acp-14-10267-2014\), 2014.](#)~~

832 McMeeking, G.R., Hamburger, T., Liu, D., Flynn, M., Morgan, W.T., Northway, M.,  
833 Highwood, E.J., Krejci, R., Allan, J.D., Minikin, A., Coe, H.: Black carbon  
834 measurements in the boundary layer over western and northern Europe. *Atmos.*  
835 *Chem. Phys.* *10*, 9393-9414, <https://doi.org/10.5194/acp-10-9393-2010>, 2010.

836 [Meng, J. W., Yeung, M. C., Li, Y. J., Lee, B. Y. L., and Chan, C. K.: Size-resolved cloud  
837 condensation nuclei \(CCN\) activity and closure analysis at the HKUST Supersite in  
838 Hong Kong, \*Atmos. Chem. Phys.\*, \*14\*, 10267–10282, \[https://doi.org/10.5194/acp-14-  
839 10267-2014\]\(https://doi.org/10.5194/acp-14-10267-2014\), 2014.](#)

840 Noureddini, H., Teoh, B. C., Davis Clements, L.: Densities of vegetable oils and fatty  
841 acids, *J. Am. Oil Chem. Soc.*, *69* (12), 1184–1188, 1992.

842 Olfert, J. S., Symonds, J. P. R., and Collings, N.: The effective density and fractal  
843 dimension of particles emitted from a light-duty diesel vehicle with a diesel oxidation  
844 catalyst, *J. Aerosol Sci.*, *38*, 69–82, <https://doi.org/10.1016/j.jaerosci.2006.10.002>,  
845 2007.

846 [Pagels, J., Khalizov, A.F., McMurry, P.H. and Zhang, R.Y.: Processing of soot by  
847 controlled sulphuric acid and water condensation-mass and mobility relationship,  
848 \*Aerosol Sci. Technol.\*, \*43\*, 629–640, <https://doi.org/10.1080/02786820902810685>,  
849 2009.](#)

带格式的: 字体颜色: 文字 1

带格式的: 字体: +西文正文 (等线), 五号, 下划线

850 Park, K., Kittelson, D. B., and McMurry, P. H.: Structural properties of diesel exhaust  
851 particles measured by transmission electron microscopy (TEM): Relationships to  
852 particle mass and mobility, *Aerosol Sci. Technol.*, 38, 881–889,  
853 <https://doi.org/10.1080/027868290505189>, 2004.

~~854 Pagels, J., Khalizov, A.F., McMurry, P.H. and Zhang, R.Y.: Processing of soot by  
855 controlled sulphuric acid and water condensation mass and mobility relationship,  
856 *Aerosol Sci. Technol.*, 43, 629–640, <https://doi.org/10.1080/02786820902810685>,  
857 2009.~~

~~858 Peng, J. F., Hu, M., Guo, S., Du, Z. F., Zheng, J., Shang, D. J., Zamora, M., Zeng, L.  
859 M., Shao, M., Wu, Y. S., Zheng, J., Wang, Y., Glen, C., Collins, D., Molina, M., and  
860 Zhang, R. Y.: Markedly enhanced absorption, and direct radiative forcing of black  
861 carbon under polluted urban environments, *P. Natl. Acad. Sci. USA*, 113(16), 4266–  
862 4271, <https://doi.org/10.1073/pnas.1602310113>, 2016.~~

863 Petters, M. D. and Kreidenweis, S. M.: A single parameter representation of  
864 hygroscopic growth and cloud condensation nucleus activity, *Atmos. Chem. Phys.*,  
865 7, 1961–1971, <https://doi.org/10.5194/acp-7-1961-2007>, 2007.

866 Paatero, P. and Tapper, U.: Positive matrix factorization: A nonnegative factormodel  
867 with optimal utilization of error estimates of data values, *Environmetrics*, 5, 111–126,  
868 1994.

~~869 Pileci, R. E., Modini, R. L., Bertò, M., Yuan, J., Corbin, J. C., Marinoni, A., Henzing,  
870 B., Moerman, M. M., Putaud, J. P., Spindler, G., Wehner, B., Müller, T., Tuch, T.,  
871 Trentini, A., Zanatta, M., Baltensperger, U., and Gysel-Beer, M.: Comparison of co-  
872 located refractory black carbon (rBC) and elemental carbon (EC) mass concentration  
873 measurements during field campaigns at several European sites, *Atmos. Meas. Tech.*,  
874 14, 1379–1403, <https://doi.org/10.5194/amt-14-1379-2021>, 2021.~~

~~875 Peng, J. F., Hu, M., Guo, S., Du, Z. F., Zheng, J., Shang, D. J., Zamora, M., Zeng, L.  
876 M., Shao, M., Wu, Y. S., Zheng, J., Wang, Y., Glen, C., Collins, D., Molina, M., and  
877 Zhang, R. Y.: Markedly enhanced absorption, and direct radiative forcing of black  
878 carbon under polluted urban environments, *P. Natl. Acad. Sci. USA*, 113(16), 4266–  
879 4271, <https://doi.org/10.1073/pnas.1602310113>, 2016.~~

880 Peng, J. F., Hu, M., Guo, S., Du, Z. F., Zheng, J., M., Zeng, L. M., Shao, M., Wu, Y. S.,  
881 Collins, D., Molina, M., and Zhang, R. Y.: Ageing and hygroscopicity variation of  
882 black carbon particles in Beijing measured by a quasi-atmospheric aerosol evolution  
883 study (QUALITY) chamber, *Atmos. Chem. Phys.*, 17(17), 10333–10348,  
884 <https://doi.org/10.5194/acp-17-10333-2017>, 2017.

885 Pan, X.L., Kanaya, Y., Taketani, F., Miyakawa, T., Inomata, S., Komazaki, Y., et al.:  
886 Emission characteristics of refractory black carbon aerosols from fresh biomass  
887 burning: a perspective from laboratory experiments, *Atmos. Chem. Phys.*, 17(21),  
888 13001–13016, <https://doi.org/10.5194/acp-17-13001-2017>, 2017.

889 Park, K., Cao, F., Kittelson, D. B., & McMurry, P. H.: Relationship between particle  
890 mass and mobility for diesel exhaust particles, *Environ. Sci. Tehnol.*, 37, 577–583,  
891 <https://doi.org/10.1021/es025960v>, 2003.

~~892 Pileci, R. E., Modini, R. L., Bertò, M., Yuan, J., Corbin, J. C., Marinoni, A., Henzing,  
893 B., Moerman, M. M., Putaud, J. P., Spindler, G., Wehner, B., Müller, T., Tuch, T.,~~

带格式的: 字体: +西文正文 (等线), 五号, 下划线

894 ~~Trentini, A., Zanatta, M., Baltensperger, U., and Gysel-Beer, M.: Comparison of co-~~  
895 ~~located refractory black carbon (rBC) and elemental carbon (EC) mass concentration~~  
896 ~~measurements during field campaigns at several European sites, Atmos. Meas. Tech.,~~  
897 ~~14, 1379–1403, <https://doi.org/10.5194/amt-14-1379-2021>, 2021.~~  
898 Qiao, K., Wu, Z., Pei, X., Liu, Q., Shang, D., Zheng, J., Du, Z., Zhu, W., Wu, Y., Lou, S.,  
899 Guo, S., Chan, C.K., Pathak, R.K., Hallquist, M., Hu, M.: Size-resolved effective  
900 density of submicron particles during summertime in the rural atmosphere of Beijing.  
901 China, J. Environ. Sci. (China) 73, 69–77. <https://doi.org/10.1016/j.jes.2018.01.012>,  
902 2018.  
903 Rissler, J., Nordin, E. Z., Eriksson, A. C., Nilsson, P. T., Frosch, M., Sporre, M. K.,  
904 Wierzbicka, A., Svenningsson, B., Londahl, J., Messing, M. E., Sjogren, S.,  
905 Hemmingsen, J. G., Loft, S., Pagels, J. H., and Swietlicki, E.: Effective Density and  
906 Mixing State of Aerosol Particles in a Near-Traffic Urban Environment, Environ. Sci.  
907 Technol., 48, 6300–6308, <https://doi.org/10.1021/es5000353>, 2014.  
908 Riemer, N., Vogel, H., and Vogel, B.: Soot aging time scales in polluted regions during  
909 day and night, Atmos. Chem. Phys., 4, 1885–1893, [https://doi.org/10.5194/acp-4-](https://doi.org/10.5194/acp-4-1885-2004)  
910 [1885-2004](https://doi.org/10.5194/acp-4-1885-2004), 2004.  
911 Ramanathan, V. and Carmichael, G.: Global and regional climate changes due to black  
912 carbon, Nat. Geosci., 36, 221–227, <https://doi.org/10.1038/ngeo156>, 2008.  
913 ~~Ren J, Zhang F, Chen L, et al.: Identifying the hygroscopic properties of fine aerosol~~  
914 ~~particles from diverse sources in urban atmosphere and the applicability in prediction~~  
915 ~~of cloud nuclei, Atmospheric Environment, 298: 119615,~~  
916 ~~<https://doi.org/10.1016/j.atmosenv.2023.119615>, 2023.~~  
917 Ren, J., Zhang, F., Wang, Y., Collins, D., Fan, X., Jin, X., et al.: Using different  
918 assumptions of aerosol mixing state and chemical composition to predict CCN  
919 concentrations based on field measurements in urban Beijing, Atmos. Chem. Phys.,  
920 18, 6907–6921, <https://doi.org/10.5194/acp-18-6907-2018>, 2018.  
921 Rader, D.J., McMurry, P.H.: Application of the tandem differential mobility analyzer  
922 to studies of droplet growth or evaporation, J. Geophys. Res.- Atmos., 17, 771–787,  
923 [https://doi.org/10.1016/0021-8502\(86\)90031-5](https://doi.org/10.1016/0021-8502(86)90031-5), 1986.  
924 Reyes-Villegas, E., Bannan, T., Le Breton, M., Mehra, A., Priestley, M., Percival, C.,  
925 Coe, H., and Allan, J. D.: Online Chemical Characterization of Food-Cooking  
926 Organic Aerosols: Implications for Source Apportionment, Environ. Sci. Technol.,  
927 52, 5308–5318, <https://doi.org/10.1021/acs.est.7b06278>, 2018.  
928 ~~Schwarz, J.P., Gao, R.S., Fahey, D.W., Thomson, D.S., Watts, L.A., Wilson, J.C.,~~  
929 ~~Reeves, J.M., Darbeheshti, M., Baumgardner, D.G., Kok, G.L., Chung, S.H., Schulz,~~  
930 ~~M., Hendricks, J., Lauer, A., Careher, B., Slowik, J.G., Rosenlof, K.H., Thompson,~~  
931 ~~T.L., Langford, A.O., Loewenstein, M., Aikin, K.C.: Single particle measurements~~  
932 ~~of midlatitude black carbon and light scattering aerosols from the boundary layer to~~  
933 ~~the lower stratosphere. J. Geophys. Res.: Atmosphere 111, D16207,~~  
934 ~~<https://doi.org/10.1029/2006JD007076>, 2006.~~  
935 Schwarz, J. P., Gao, R. S., Spackman, J. R., Watts, L. A., Thomson, D. S., Fahey, D.  
936 W., Ryerson, T. B., Peischl, J., Holloway, J. S., Trainer, M., Frost, G. J., Baynard,  
937 T., Lack, D. A., de Gouw, J. A., Warneke, C., and Del Negro, L. A.: Measurement

带格式的: 超链接, 字体: +西文正文(等线), 五号

938 of the mixing state, mass, and optical size of individual black carbon particles in  
939 urban and biomass burning emissions, *Geophys. Res. Lett.*, 35, L13810,  
940 <https://doi.org/10.1029/2008GL033968>, 2008.

~~941 Stokes, R. and Robinson, R.: Interactions in aqueous nonelectrolyte solutions. I. Solute-~~  
~~942 solvent equilibria, *J. Phys. Chem.-US*, 70, 2126–2131, 1966.~~

943 Sun, Y., Du, W., Fu, P., Wang, Q., Li, J., Ge, X., Zhang, Q., Zhu, C., Ren, L., Xu, W.,  
944 Zhao, J., Han, T., Worsnop, D. R., and Wang, Z.: Primary, and secondary aerosols  
945 in Beijing in winter: sources, variations, and processes, *Atmos. Chem. Phys.*, 16,  
946 8309–8329, <https://doi.org/10.5194/acp-16-8309-2016>, 2016.

~~947 Sun, Y. L., Wang, Z. F., Du, W., Zhang, Q., Wang, Q. Q., Fu, P. Q., Pan, X. L., Li, J.,~~  
~~948 Jayne, J., and Worsnop, D. R.: Long-term real-time measurements of aerosol particle~~  
~~949 composition in Beijing, China: seasonal variations, meteorological effects, and~~  
~~950 source analysis, *Atmos. Chem. Phys.*, 15, 10149–10165, [https://doi.org/10.5194/acp-](https://doi.org/10.5194/acp-15-10149-2015)~~  
~~951 [15-10149-2015](https://doi.org/10.5194/acp-15-10149-2015), 2015.~~

~~952 Stokes, R. and Robinson, R.: Interactions in aqueous nonelectrolyte solutions. I. Solute-~~  
~~953 solvent equilibria, *J. Phys. Chem.-US*, 70, 2126–2131, 1966.~~

~~954 Schwarz, J.P., Gao, R.S., Fahey, D.W., Thomson, D.S., Watts, L.A., Wilson, J.C.,~~  
~~955 Reeves, J.M., Darbeheshti, M., Baumgardner, D.G., Kok, G.L., Chung, S.H., Schulz,~~  
~~956 M., Hendricks, J., Lauer, A., K€archer, B., Slowik, J.G., Rosenlof, K.H., Thompson,~~  
~~957 T.L., Langford, A.O., Loewenstein, M., Aikin, K.C.: Single-particle measurements~~  
~~958 of midlatitude black carbon and light-scattering aerosols from the boundary layer to~~  
~~959 the lower stratosphere. *J. Geophys. Res.: Atmosphere* 111, D16207,~~  
~~960 <https://doi.org/10.1029/2006JD007076>, 2006.~~

961 Shiraiwa, M., Kondo, Y., Moteki, N., Takegawa, N., Sahu, L., Takami, A., et al.:  
962 Radiative impact of mixing state of black carbon aerosol in Asian outflow, *J.*  
963 *Geophys. Res.- Atmos.*, 113, D24210, <https://doi.org/10.1029/2008JD010546>, 2008.

964 Tan, H., Xu, H., Wan, Q., Li, F., Deng, X., Chan, P. W., Xia, D., and Yin, Y.: Design  
965 and application of an unattended multifunctional H-TDMA system, *J. Atmos. Ocean.*  
966 *Tech.*, 30, 1136–1148, <https://doi.org/10.1175/JTECH-D-12-00129.1>, 2013.

967 Ulbrich, I. M., Canagaratna, M. R., Zhang, Q., Worsnop, D. R., and Jimenez, J. L.:  
968 Interpretation of organic components from Positive Matrix Factorization of aerosol  
969 mass spectrometric data, *Atmos. Chem. Phys.*, 9, 2891–2918,  
970 <https://doi.org/10.5194/acp-9-2891-2009>, 2009.

971 Wang, Y., Wan, Q., Meng, W., Liao, F., Tan, H., and Zhang, R.: Long-term impacts of  
972 aerosols on precipitation and lightning over the Pearl River Delta megacity area in  
973 China, *Atmos. Chem. Phys.*, 11, 12421–12436, [https://doi.org/10.5194/acp-11-](https://doi.org/10.5194/acp-11-12421-2011)  
974 [12421-2011](https://doi.org/10.5194/acp-11-12421-2011), 2011.

975 Wang, Y. Y., Liu, F. S., He, C. L., Bi, L., Cheng, T. H., Wang, Z. L., Zhang, H., Zhang,  
976 X. Y., Shi, Z. B., and Li, W. J.: Fractal dimensions and mixing structures of soot  
977 particles during atmospheric processing, *Environ. Sci. Tech. Lett.*, 4, 487–493,  
978 <https://doi.org/10.1021/acs.estlett.7b00418>, 2017.

979 Wu, Y. F., Xia, Y. J., Huang, R. J., Deng, Z. Z., Tian, P., Xia, X. G., et al.: A study of the  
980 morphology and effective density of externally mixed black carbon aerosols in  
981 ambient air using a size-resolved single-particle soot photometer (SP2), *Atmos. Meas.*

982 Tech., 12, 4347–4359, <https://doi.org/10.5194/amt-12-4347-2019>, 2019.

983 Wu, Y., Wang, X., Tao, J., Huang, R., Tian, P., Cao, J., Zhang, L., Ho, K.-F., Han, Z.,  
984 and Zhang, R.: Size distribution and source of black carbon aerosol in urban Beijing  
985 during winter haze episodes, *Atmos. Chem. Phys.*, 17, 7965–7975,  
986 <https://doi.org/10.5194/acp-17-7965-2017>, 2017.

987 Wu, Z. J., Zheng, J., Shang, D. J., Du, Z. F., Wu, Y. S., Zeng, L. M., Wiedensohler, A.,  
988 and Hu, M.: Particle hygroscopicity and its link to chemical composition in the urban  
989 atmosphere of Beijing, China, during summertime, *Atmos. Chem. Phys.*, 16, 1123–  
990 1138, <https://doi.org/10.5194/acp-16-1123-2016>, 2016.

991 Xue, H., Khalizov, A. F., Wang, L., Zheng, J., and Zhang, R.: Effects of dicarboxylic  
992 acid coating on the optical properties of soot, *Phys. Chem. Chem. Phys.*, 11, 7869–  
993 7875, <https://doi.org/10.1039/b904129j>, 2009.

994 Xu, W., Sun, Y., Wang, Q., Zhao, J., Wang, J., Ge, X., et al.: Changes in aerosol  
995 chemistry from 2014 to 2016 in winter in Beijing: Insights from high-resolution  
996 aerosol mass spectrometry, *J. Geophys. Res.-Atmos.*, 124, 1132–1147.  
997 <https://doi.org/10.1029/2018jd029245>, 2019.

998 ~~Xu, W., Fossom, K. N., Ovadnevaite, J., Lin, C., Huang, R. J., O'Dowd, C., and~~  
999 ~~Ceburnis, D.: The impact of aerosol size dependent hygroscopicity and mixing state~~  
1000 ~~on the cloud condensation nuclei potential over the north-east Atlantic, *Atmos. Chem.*~~  
1001 ~~*Phys.*, 21, 8655–8675, <https://doi.org/10.5194/acp-21-8655-2021>, 2021.~~

1002 Yuan, T., Li, Z., Zhang, R., and Fan, J.: Increase of cloud droplet size with aerosol  
1003 optical depth: An observation and modeling study, *J. Geophys. Res.-Atmos.*, 113,  
1004 D04201, <https://doi.org/10.1029/2007JD008632>, 2008.

1005 Yu, C., Liu, D., Broda, K., Joshi, R., Olfert, J., Sun, Y., Fu, P., Coe, H., Allan, J.D.:  
1006 Characterising mass-resolved mixing state of black carbon in Beijing using a  
1007 morphology-independent measurement method, *Atmos. Chem. Phys.*, 20, 3645–  
1008 3661. <https://doi.org/10.5194/acp-20-3645-2020>, 2020.

1009 Zhang, R. Y., Khalizov, A. F., Pagels, J., Zhang, D., Xue, H. X., and McMurry, P. H.:  
1010 Variability in morphology, hygroscopicity, and optical properties of soot aerosols  
1011 during atmospheric processing, *P. Natl. Acad. Sci. USA*, 105, 10291–10296,  
1012 <https://doi.org/10.1073/pnas.0804860105>, 2008.

1013 ~~Zhang, F., Li, Z., Li, Y., Sun, Y., Wang, Z., Li, P., Sun, L., Wang, P., Cribb, M., Zhao,~~  
1014 ~~C., Fan, T., Yang, X., and Wang, Q.: Impacts of organic aerosols and its oxidation~~  
1015 ~~level on CCN activity from measurement at a suburban site in China, *Atmos. Chem.*~~  
1016 ~~*Phys.*, 16, 5413–5425, <https://doi.org/10.5194/acp-16-5413-2016>,~~  
1017 ~~2016a.~~

1018 ~~Zhang, Cheng, Y., Su, H., Kecorius, S., Wang, Z., Wu, Z., Hu, M., Zhu, T.,~~  
1019 ~~Wiedensohler, A., and He, K.: Measuring the morphology and density of internally~~  
1020 ~~mixed black carbon with SP2 and VTDMA: new insight into the absorption~~  
1021 ~~enhancement of black carbon in the atmosphere, *Atmos. Meas. Tech.*, 9, 1833–1843,~~  
1022 ~~<https://doi.org/10.5194/amt-9-1833-2016>, 2016.~~

1023 ~~Zdanovskii, A.: New methods for calculating solubilities of electrolytes in~~  
1024 ~~multicomponent systems, *Zh. Fiz. Khim.*, 22, 1475–1485, 1948.~~

1025 ~~Zhang, F., Wang, Y., Peng, J., Ren, J., Collins, D., Zhang, R., et al.: Uncertainty in~~

带格式的: 超链接, 字体: +西文正文 (等线), 五号

带格式的: 超链接, 字体: +西文正文 (等线), 五号

带格式的: 超链接, 字体: +西文正文 (等线), 五号

带格式的: 字体颜色: 自动设置



1026 predicting CCN activity of aged and primary aerosols, *J. Geophys. Res.-Atmos.*,  
1027 122(21), 11723–11736, <https://doi.org/10.1002/2017jd027058>, 2017.

1028 Zhang, F., Ren, J., Fan, T., Chen, L., Xu, W., Sun, Y., et al.: Significantly enhanced  
1029 aerosol CCN activity and number, *J. Geophys. Res.-Atmos.*, 124, 14102–14113,  
1030 <https://doi.org/10.1029/2019jd031457>, 2019.

1031 Zhang, F., Wang, Y., Peng, J., Chen, L., Sun, Y., Duan, L., Ge, X., Li, Y., Zhao, J., Liu,  
1032 C., Zhang, X., Zhang, G., Pan, Y., Wang, Y., Zhang, A. L., Ji, Y., Wang, G., Hu, M.,  
1033 Molina, M. J., Zhang, R.: An unexpected catalyst dominates formation and radiative  
1034 forcing of regional haze, *P. Natl. Acad. Sci. USA*, 117(8), 3960–3966,  
1035 <https://doi.org/10.1073/pnas.1919343117>, 2020a.

1036 Zhang, Y., Zhang, Q., Cheng, Y., Su, H., Kecorius, S., Wang, Z., Wu, Z., Hu, M., Zhu,  
1037 T., Wiedensohler, A., and He, K.: Measuring the morphology and density of  
1038 internally mixed black carbon with SP2 and VTDMA: new insight into the  
1039 absorption enhancement of black carbon in the atmosphere, *Atmos. Meas. Tech.*, 9,  
1040 1833–1843, <https://doi.org/10.5194/amt-9-1833-2016>, 2016b.

1041 Yao, Z., Li, H.: Particle Size and Mixing State of Freshly Emitted Black Carbon from  
1042 Different Combustion Sources in China, *Environ. Sci. Technol.*, 54(13): p. 7766–  
1043 7774, <https://doi.org/10.1021/acs.est.9b07373>, 2020b.

1044 Zhang, F., Peng, J., Chen, L., Collins, D., Li, Y., Jiang, S., Liu, J., Zhang, R.: The effect  
1045 of Black carbon aging from NO<sub>2</sub> oxidation of SO<sub>2</sub> on its morphology, optical and  
1046 hygroscopic properties, *Environ. Res.*, 212, 113238,  
1047 <https://doi.org/10.1016/j.envres.2022.113238>, 2022.

1048 Zhang, R., Wang, G., Guo, S., Zamora, M. L., Ying, Q., Lin, Y.: Formation of urban  
1049 fine particulate matter, *Chemical Reviews*, 115(10), 3803–3855,  
1050 <https://doi.org/10.1021/acs.chemrev.5b00067>, 2015.

1051 Zhou, Y., Ma, N., Wang, Q., Wang, Z., Chen, C., Tao, J., Hong, J., Peng, L., He, Y.,  
1052 Xie, L., Zhu, S., Zhang, Y., Li, G., Xu, W., et al.: Bimodal distribution of size-  
1053 resolved particle effective density: results from a short campaign in a rural environ-  
1054 ment over the North China Plain, *Atmos. Chem. Phys.*, 22, 2029–2047,  
1055 <https://doi.org/10.5194/acp-22-2029-2022>, 2022.

1056 Zhao, G., Tan, T., Hu, S., Du, Z., Shang, D., Wu, Z., Guo, S., Zheng, J., Zhu, W., Li,  
1057 M., Zeng, L., and Hu, M.: Mixing state of black carbon at different atmospheres in  
1058 north and southwest China, *Atmos. Chem. Phys.*, 22, 10861–10873,  
1059 <https://doi.org/10.5194/acp-22-10861-2022>, 2022.

1060 Zhang, F., Ren, J., Fan, T., Chen, L., Xu, W., Sun, Y., et al.: Significantly enhanced  
1061 aerosol CCN activity and number, *J. Geophys. Res.-Atmos.*, 124, 14102–14113,  
1062 <https://doi.org/10.1029/2019jd031457>, 2019.

1063 Zdanovskii, A.: New methods for calculating solubilities of electrolytes in  
1064 multicomponent systems, *Zh. Fiz. Khim.*, 22, 1475–1485, 1948.

1065 Zhang, R., Wang, G., Guo, S., Zamora, M. L., Ying, Q., Lin, Y.: Formation of urban  
1066 fine particulate matter, *Chemical Reviews*, 115(10), 3803–3855,  
1067 <https://doi.org/10.1021/acs.chemrev.5b00067>, 2015.

1068 Zhang, Y., Zhang, Q., Yao, Z., Li, H.: Particle Size and Mixing State of Freshly Emitted  
1069 Black Carbon from Different Combustion Sources in China, *Environ. Sci. Technol.*,  
1070 54(13): p. 7766–7774, <https://doi.org/10.1021/acs.est.9b07373>, 2020b.

带格式的: 默认段落字体, 字体: +西文正文(等线), 五号, 下划线, 字体颜色: 自动设置

带格式的: 默认段落字体, 字体: +西文正文(等线), 五号, 下划线, 字体颜色: 自动设置

带格式的: 下划线

带格式的: 默认段落字体, 字体: +西文正文(等线), 五号, 下划线, 字体颜色: 自动设置

带格式的: 字体颜色: 自动设置

带格式的: 不对齐到网格